JOC The Journal of Organic Chemistry

Article

Effects of the Distance Between Radical Sites on the Reactivities of Aromatic Biradicals

Duanchen Ding, Hanning Jiang, Xin Ma, John J. Nash, and Hilkka I. Kenttämaa

J. Org. Chem., **Just Accepted Manuscript** • DOI: 10.1021/acs.joc.0c00658 • Publication Date (Web): 01 Jun 2020

is published by the American Chemical Society. 1155 Sixteenth Street N.W., Washington, DC 20036

Effects of the Distance Between Radical Sites on the Reactivities of Aromatic Biradicals

Duanchen Ding, Hanning Jiang, Xin Ma, John J. Nash, and Hilkka I. Kenttämaa*

Department of Chemistry, Purdue University, 560 Oval Drive,

West Lafayette, Indiana, 47907

*Corresponding author: Professor Hilkka I. Kenttämaa, Email: hilkka@purdue.edu, Telephone: +1 (765) 494−0882.

ABSTRACT: Coupling of the radical sites in the isomeric benzynes is known to hinder their radical reactivity. In order to determine how far apart the radical sites must be for them not to interact, the gas-phase reactivity of several isomeric protonated (iso)quinoline-and acridine-based biradicals was examined. All the (iso)quinolinium-based biradicals were found to react slower than related monoradicals with similar vertical electron affinities (i.e., similar polar effects). In sharp contrast, the acridinium-based biradicals, most with the radical sites farther apart than in the (iso)quinolinium-based systems, showed greater reactivities than the relevant monoradicals with similar vertical electron affinities. The greater distances between the two radical sites in these biradicals lead to very little or no spin-spin coupling, and no suppression of radical reactivity was observed. Therefore, the radical sites can still interact if they are located on adjacent benzene rings and only after being separated further than that does no coupling occur. The most reactive radical site of each biradical was experimentally determined to be the one predicted to be more reactive based on the monoradical reactivity data. Therefore, the calculated vertical electron affinities of relevant monoradicals can be used to predict which radical site is most reactive in the biradicals.

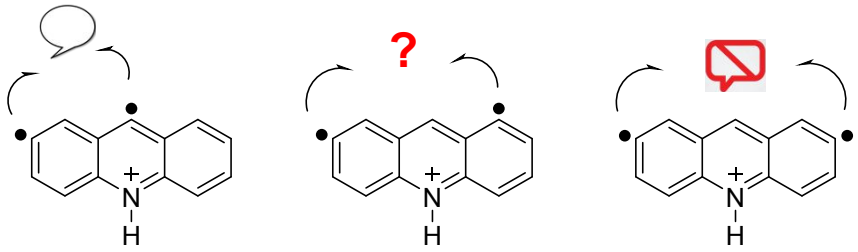

Table of Contents Graphic

INTRODUCTION

σ-Type carbon-centered aromatic biradicals, including the three benzynes (*ortho*-, *meta*- and *para*-) and their analogs, have been studied for decades for their potential applications in various fields, including organic synthesis and anticancer therapeutics.[1-8] Due to the difficulty of cleanly and *simultaneously* generating two radical sites that are not adjacent to each other in solution, mass spectrometers have been used to study numerous gas-phase aromatic biradicals with a chemically inert charged site.[5,7,8] These biradicals are generated from protonated diiodo- or iodonitroprecursors by using collision-activated dissociation to homolytically cleave off iodo atoms and/or nitro goups. In most cases, the charged site has been demonstrated to influence reactions like a strongly electron-withdrawing substituent, without directly participating in the reactions.[9]

In previous studies, several factors have been elucidated that control the chemical behavior of the types of mono- and biradicals described above. For instance, the (calculated) vertical electron affinity (EA_v) of the radical site(s) plays a significant role in controlling the reaction efficiencies of polar mono- and biradicals.[5,7,9-11] The reactivities of a series of quinolinium-based monoradicals toward cyclohexane and allyl iodide have been reported to increase with increasing EA_v (Table 1).[11] A relatively high EA_v helps stabilize a polar resonance structure of the transition state for radical reactions, which has been proposed to increase reactivity.[7,9,12] Specifically, for monoradicals, the natural logarithm of the H atom abstraction reaction efficiency has been reported to linearly correlate with the (calculated) EA_v.[9] It should be noted here that based on recent literature, a designated local electric field created by charged functional groups can influence reaction rates via field effects and the alignment of the field parallel to the reacting center causes the greatest effect.[13] However, although monoradicals **q2** and **q6** have very different orientations between the N-H polar bond and the radical orbital (aligned for **q2** but orthogonal for **q6**), which suggest that **q2** should experience much stronger field effects, these radicals yield exactly the same products with the same branching ratios and also react at the same efficiency with both cyclohexane and allyl iodide. These results suggest that the relative orientation of the most polar bond and the radical orbital does not play a major role in the systems studied here. This may be due to the delocalization of the charge in these systems as the field effects have

Table 1. Reaction Efficiencies[a] and Observed Reactions[b] With Branching Ratios[c] for Quinolinium-based Monoradicals Upon Interaction with Cyclohexane and Allyl Iodide, and Calculated[d] Vertical Electron Affinities (EA_v)[11]

Monoradicals	 **q1**		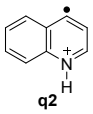 **q2**		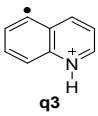 **q3**		 **q4**		 **q5**		 **q6**	
EA_v (eV)	6.30		5.59		5.06		4.74		4.89		5.51	
Cyclohexane	H abs	100%	H abs	100%	H abs	100%	H abs	100%	H abs	100%	H abs	100%
	Efficiency = 36%		**Efficiency = 14%**		**Efficiency = 3%**		**Efficiency = 1%**		**Efficiency = 1%**		**Efficiency = 12%**	
Allyl Iodide	I abs	85%	I abs	94%	I abs	97%	I abs	93%	I abs	92%	I abs	96%
	Allyl abs	15%	Allyl abs	6%	Allyl abs	3%	Allyl abs	7%	Allyl abs	8%	Allyl abs	4%
	Efficiency = 64%		**Efficiency = 54%**		**Efficiency = 38%**		**Efficiency = 30%**		**Efficiency = 25%**		**Efficiency = 56%**	

[a]Percentage of collisions that lead to reaction; k_{exp}/k_{coll} (reaction rate constant / calculated collision rate constant) × 100. [b]abs = abstraction. [c]Branching ratios of primary reactions were determined by dividing the abundance of the product ion by the sum of the abundances of all product ions. [d]Calculated at the CASPT2/CASSCF(12,11)/cc-pVTZ//UB3LYP/cc-pVTZ level of theory.

been proposed to be weaker in more delocalized ions.[13] Furthermore, they have also been proposed to be weaker for ions with a localized radical site,[13] which applies to the systems discussed here.

Additional parameters control the reactivities of related biradicals. For example, most of the reported biradicals have singlet ground states.[7,11,14] In the transition states of radical reactions of biradicals, some extra energy (i.e., compared to a monoradical) is required to partially uncouple the two nonbonding electrons.[15] The extra energy required has been proposed to be related to the magnitude of the singlet-triplet splitting ($\Delta E_{S\text{-}T}$), which reflects the strength of the spin-spin coupling between the two radical sites.[7,11,14] For example, *ortho*-benzyne has been measured[6] to have a $\Delta E_{S\text{-}T}$ of −37.5 kcal mol^{-1} (the negative sign indicates a singlet ground state), which indicates very strong spin-spin coupling that should prevent radical reactivity.[4,16] Indeed, a quinolinium-based *ortho*-benzyne, the 2-pyridyl cation (see Chart 1), has been reported not to undergo radical reactions.[17] In contrast, the 4,5-didehydroisoquinolinium cation (**i1**; Chart 2), which has a calculated $\Delta E_{S\text{-}T}$ of –1.3 kcal mol^{-1}, shows relatively high radical reactivity.[8,14] In addition to (or in place of)

Chart 1. The 2-pyridyl cation.

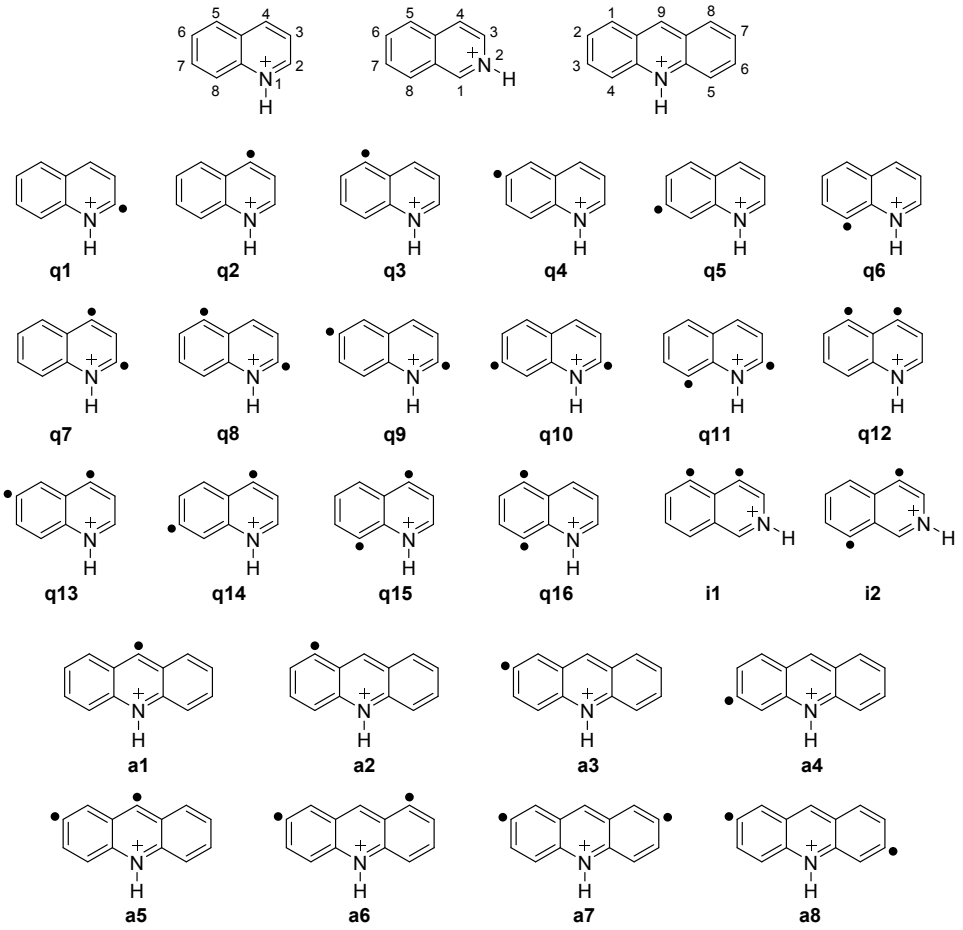

Chart 2. Numbering schemes for **q**uinolinium, **i**soquinolinium, and **a**cridinium systems, and the mono- and biradicals studied.

EA_v and ΔE_{S-T}, the reactivities of *meta*-benzynes have been demonstrated to depend on at least three different reactivity-controlling parameters, i.e., the enthalpy required to distort the minimum energy dehydrocarbon atom separation to the separation of the transition state and the ΔE_{S-T} and EA_v values at the dehydrocarbon atom separation of the transition state.[7]

The orientations of the nonbonding orbitals and the distances between them in benzynes have been shown to affect their spin-spin coupling strength[6,18] and thereby their reactivity.[4,5] However, the effects of these parameters on the reactivity of other related biradicals have not been studied. In an effort to determine how far apart the two radical sites must be for them not to interact at all, a series of (iso)quinolinium- and acridinium-based biradicals (Chart 1) were generated (from the precursors shown in Chart 3) and allowed to react with cyclohexane and allyl iodide in the gas phase in a quadrupole ion trap mass spectrometer. Related monoradicals have been reported to react with these reagents in the gas phase via simple radical pathways – H or I atom abstraction, respectively.[10,11,14] A kinetic reactivity study was carried out and the results were compared with those obtained for related monoradicals[11] and those previously reported[8,11,14] for (iso)quinolinium-based biradicals. The experiments were complemented by quantum chemical calculations.

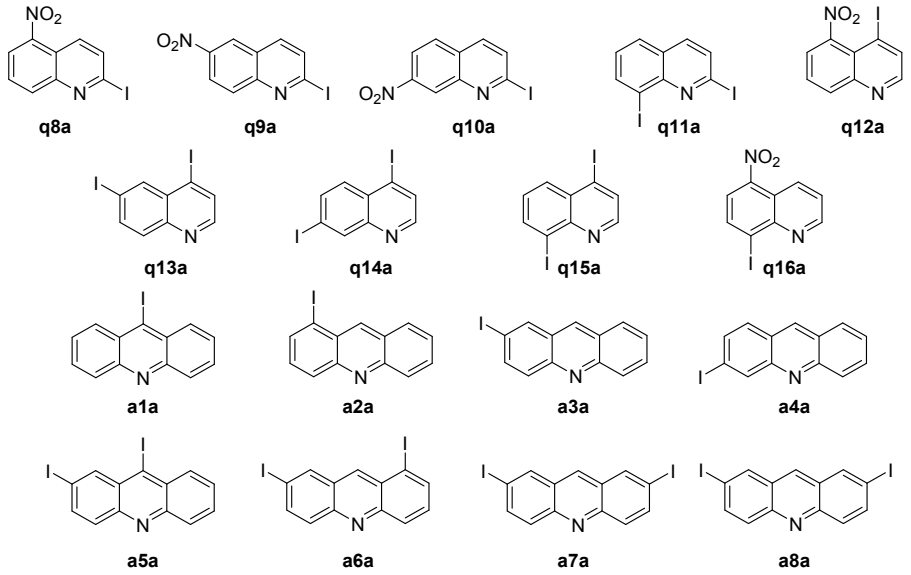

Chart 3. Precursors for quinolinium- and acridinium-based radicals used in this study.

RESULTS AND DISCUSSION

The experimental design that was chosen for the comparison of the relative reactivities of different biradicals, or more accurately, the relative activation enthalpies ($\Delta H^{\ddagger}_{act}$) of reactions of different biradicals, is as follows. The efficiencies of H or I atom abstraction reactions by charged biradicals from cyclohexane or allyl iodide, respectively, were determined by multiplying the measured total reaction efficiencies (number of reactive collisions divided by the number of all collisions) with the measured branching ratios of the H or I atom abstraction reaction to obtain a measure of the rate of the radical reaction vs the rate of dissociation back to reactants. These radical reactions are highly exothermic (for example, -16 kcal mol^{-1} for abstraction of a H atom by biradical **q13** (Chart 2) at either radical site from cyclohexane, as calculated at the (U)M06-2X//6-

311++G(d,p) level of theory; the corresponding Gibbs free energy calculated at the same level of theory is -18 kcal mol^{-1}) and irreversible (see Figure 1 for a schematic of a Brauman double-well

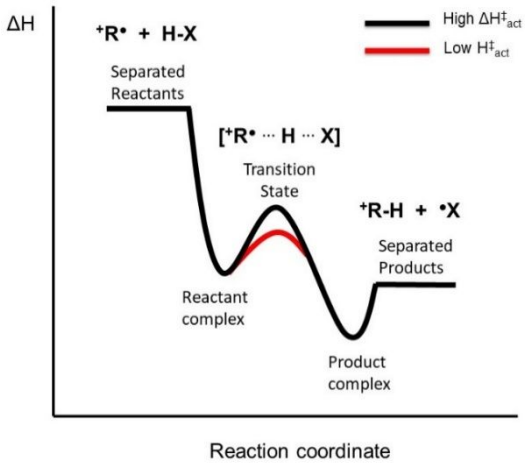

Figure 1. Brauman double-well potential energy surface for H atom abstraction by a charged monoradical ($^{+}R^{\bullet}$) from a hypothetical H atom donor HX in the gas phase. Two reactions are depicted, one with a higher $\Delta H^{\ddagger}_{act}$ and another one with a lower $\Delta H^{\ddagger}_{act}$ (red color).

potential energy surface[19]). Therefore, the measured relative H and I atom abstraction efficiencies reflect the relative $\Delta H^{\ddagger}_{act}$ of these reactions.

(Iso)Quinolinium-based biradicals. The observed reactions and the reaction efficiencies measured for the (iso)quinolinium-based biradicals upon interactions with cyclohexane and allyl iodide, along with the calculated EA_v and $\Delta E_{S\text{-}T}$ values of the biradicals, are shown in Table 2. The data for the 2,4-didehydroquinolinium cation (**q7**) have been reported previously[11] (the same results were obtained in this study). The EA_v and $\Delta E_{S\text{-}T}$ values of the 4,6-didehydroquinolinium (**q13**) and 4,7-didehydroquinolinium (**q14**) cations have been calculated before.[10] In the same study, their reaction efficiencies with cyclohexane were determined to be 2% and 4%, respectively.[10] Quite different results were obtained in this study (Table 2). The exact reason for this discrepancy is not known at this time but the values reported here were found to be highly reproducible, which was not true for the previously reported values.

Similar to the quinolinium-based monoradicals (Table 1), all biradicals reacted via predominant (primary) H atom abstraction with cyclohexane (followed by abstraction of a second H atom from a different cyclohexane molecule in a secondary reaction). Additional, mostly slow, reactions that were observed include hydride abstraction from cyclohexane by the biradical (H^{-} abs; Table 2), formation of a stable adduct between the biradical and cyclohexane (addition), and nominal addition of cyclohexane to the biradical followed by elimination of a H atom (addition-H) (Scheme 1).

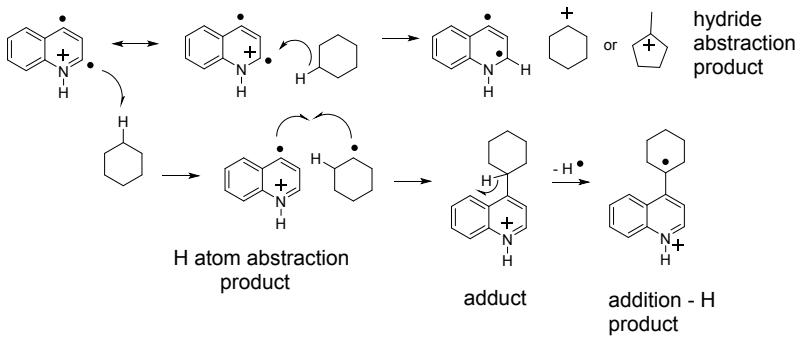

Scheme 1. Different reaction pathways for biradical **q7** and cyclohexane.

Upon reactions with allyl iodide, most of the biradicals showed I atom abstraction (followed by a second I atom abstraction from a different allyl iodide molecule) as the major reaction, which is consistent with the behavior observed for the monoradicals. The abstraction of two H atoms from cyclohexane and two I atoms from allyl iodide confirmed the presence of two radical sites for each biradical.

Surprisingly, most biradicals showed a larger proportion of allyl group abstraction than the monoradicals (the same observation was made for the acridinium-based biradicals; see below), and the *meta*-benzyne, **q7**, *para*-benzyne, **q16**, and the 2,8-didehydroquinolinium cation, **q11**, exhibited dominant allyl group abstraction. This behavior is not characteristic for *meta*- and *para*-benzynes as not all *meta*- and *para*-benzynes described in the literature show similar behavior.[20,21] It should also be noted that the ions expected to be **q11** may, in fact, be a mixture of isomers. When the monoradical precursor of this biradical, the 8-dehydro-2-iodoquinolinium cation, is subjected to CAD to generate the second radical site, the H atom at N−1 may migrate to C−8 to ultimately form an *ortho*-benzyne isomer of **q11**. A similar type of rearrangement has been reported[20] for the

Table 2. Total Reaction Efficiencies,[a] Observed Reactions[b,c] With Branching Ratios,[d] and H and I Atom Abstraction Efficiencies[c] for Quinolinium-based Biradicals Upon Interaction with Cyclohexane and Allyl Iodide, Together With the Calculated[e] Vertical Electron Affinities (EA_v) and Singlet-Triplet Splittings (ΔE_{S-T}) of the Biradicals

Biradicals	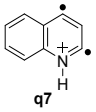 q7	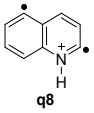 q8	 q9	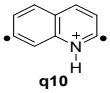 q10	 q11	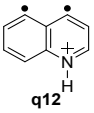 q12
EA_v (eV)	6.21 (at DAS[f] 2.3 Å)	6.39	6.37	6.31	6.38	5.61
ΔE_{S-T} (kcal mol^{-1})	−26.4 $\Delta E_{2.3}$[g]: 8.5 kcal mol^{-1}	−0.3	−0.7	−2.6	−0.8	-1.1
Cyclohexane	H abs 50% 2° H abs Addition – H 42% Addition 8% **Efficiency = 0.4%** **H abs eff. = 0.2%**	H abs 87% 2° H abs Addition 9% H⁻ abs 4% **Efficiency = 36%** **H abs eff. = 31%** URI[h] = 52%[e]	H abs 88% 2° H abs Addition 9% H⁻ abs 3% **Efficiency = 34%** **H abs eff. = 30%** URI = 55%	H abs 74% 2° H abs Addition 21% H⁻ abs 4% **Efficiency = 30%** **H abs eff. = 22%** URI = 66%	H abs 71% 2° H abs Addition 10% Addition – H 13% H⁻ abs 6% **Efficiency = 31%** **H abs eff. = 22%** URI = 85%	H abs 64% 2° H abs Addition 28% H⁻ abs 8% **Efficiency = 9%** **H abs eff. = 6%** URI = 78%
Allyl Iodide	Allyl abs 83% 2° I abs I abs 9% 2° allyl abs Allene abs 8% **Efficiency = 0.9%** **I abs eff. = 0.08%**	I abs 63% 2° I abs Allyl abs 31% 2° I abs 2° Allyl abs Allene abs 7% **Efficiency = 80%** **I abs eff. = 50%** URI = 53%	I abs 64% 2° I abs Allyl abs 33% 2° I abs Allene abs 4% **Efficiency = 80%** **I abs eff. = 51%** URI = 57%	I abs 55% 2° I abs Allyl abs 36% 2° I abs 2° Allyl abs Allene abs 9% **Efficiency = 76%** **I abs eff. = 42%** URI = 73%/	Allyl abs 59% 2° I abs Allene abs 21% I abs 21% 2° I abs **Efficiency = 63%** **I abs eff. = 13%** URI = 86%	I abs 77% 2° I abs Allyl abs 10% Adduct 7% Allene abs 3% **Efficiency = 55%** **I abs eff. = 42%** URI = 63%

Biradicals[i]	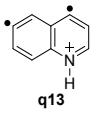 q13	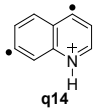 q14	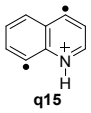 q15	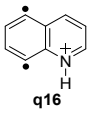 q16	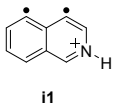 i1	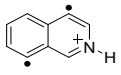 i2
EA_v (eV)	5.67	5.68	5.56	5.50	5.70	5.53
ΔE_{S-T} (kcal mol^{-1})	−1.1	−0.3	-8.3	−4.2	-1.3	-8.1
Cyclohexane	H abs 78% 2° H abs Addition 16% H⁻ abs 5% **Efficiency = 13%** **H abs eff. = 10%** URI = 52%	H abs 85% 2° H abs Addition 12% H⁻ abs 3% **Efficiency = 15%** **H abs eff. = 13%** URI = 54%	H abs 51% 2° H abs Addition 32% H⁻ abs 7% **Efficiency = 8%** **H abs eff. = 4%** URI = 76%	H abs 99% 2° H abs Addition 1% **Efficiency = 1%** **H abs eff. = 1%** URI = 47%	2 x H abs 46% H abs 35% 2° H abs Addition 19% **Efficiency = 18%** **H abs eff. = 7%**	H abs 49% 2° H abs 2 x H abs 30% Addition 21% **Efficiency = 2%** **H abs eff. = 1%**
Allyl Iodide	I abs 81% 2° I abs Allyl abs 15% 2° I abs Allene abs 4% **Efficiency = 53%** **I abs eff. = 43%** URI = 48%	I abs 79% 2° I abs Allyl abs 17% 2° I abs Allene abs 4% **Efficiency = 54%** **I abs eff. = 43%** URI = 48%	I abs 76% 2° I abs Allyl abs 22% 2° I abs Allene abs 2% **Efficiency = 42%** **I abs eff. = 32%** URI = 83%	Allyl abs 80% 2° I abs Allene abs 15% I abs 5% **Efficiency = 4%** **I abs eff. = 0.2%** URI = 92%	I abs 58% 2° I abs 2° Allyl abs Allene abs 42% **Efficiency = 42%** **I abs eff. = 24%**	I abs 92% 2° I abs 2° Allyl abs Allene abs 8% **Efficiency = 41%** **I abs eff. = 38%**

[a] % collisions that lead to reaction; k_{exp}/k_{coll} (reaction rate constant/calculated collision rate constant) ×100. [b]abs = abstraction. [c]H and I atom abstraction efficiencies calculated by multiplying the total reaction efficiency with the branching ratio of H atom abstraction from cyclohexane or I atom abstraction from allyl iodide. 2° H (or I or allyl) abs implies that this H abs is a secondary reaction of the product shown just above. The identity of the primary product that produced each secondary product was deduced from the rate plots prepared for all studied reactions. When not clear, each primary product ion was isolated and its reactions examined. [d]Branching ratios of primary reactions were determined by dividing the abundance of the product ion by the sum of the abundances of all product ions. [e]ΔE_{S-T} values calculated at the CASPT2/CASSCF(12,12)/cc-pVTZ//UB3LYP/cc-pVTZ level of theory; EA_v values calculated at the CASPT2/CASSCF(13,12)/cc-pVTZ//UB3LYP/cc-pVTZ level of theory. [f]DAS = dehydrocarbon atom separation. [g]$\Delta E_{2.3}$ is defined as the energy required for the *meta*-benzyne to reach the transition state geometry with a DAS of 2.3 Å from the minimum-energy geometry of the (ground) singlet state (ref. 7). [h]URI = unreactive isomer; the structures of the unreactive isomers are unknown in most cases; the percentage of URI was determined from the rate plots at long reaction times. [i]Data for **i1** and **i2** from ref. 14.

analogous 5-iodo-8-dehydroquinolinium monoradical that partially undergoes migration of the H atom at N−1 to C−8 upon the second CAD step. Elimination of the I atom then results in a mixture of isomers: the 5,8-didehydroquinolinium cation and its *ortho*-isomer. This mixture showed major allyl abstraction instead of I atom abstraction upon reaction with allyl iodide.[20]

Perhaps not surprisingly, no correlations were found between the reactivities (i.e., reaction efficiencies) of the biradicals studied here and either their $\Delta E_{S\text{-}T}$ or EA_v values (individually) (Figures 1, 2 and S1). This was the case when comparing either the total reaction efficiencies for cyclohexane and allyl iodide, or the reaction efficiencies for H atom abstraction from cyclohexane or I atom abstraction from allyl iodide. Indeed, the radical reactivity of *meta*-benzynes[7] has been shown to depend on at least three variables: (1) the energy required to distort the minimum energy dehydrocarbon atom separation to the separation of the transition state and (2) the $\Delta E_{S\text{-}T}$ and (3) the EA_v values at the dehydrocarbon atom separation of the transition state (dehydrocarbon atom separation of 2.3 Å). Only the reactivity of **q7** (a *meta*-benzyne) would be expected to be affected by distortion energy, but *both* EA_v and $\Delta E_{S\text{-}T}$, and possibly additional factors, should influence the reactivities of all the other biradicals studied here.

Most of the studied biradicals showed lower total reaction efficiencies relative to the monoradicals with a similar EA_v. For example, the 4,8-didehydroquinolinium cation (**q15**) is less reactive toward cyclohexane and allyl iodide (efficiencies = 8% and 42%, respectively; Table 2) than the related monoradicals, **q2** (efficiencies = 14% (cyclohexane) and 54% (allyl iodide)) and **q6** (efficiencies = 12% (cyclohexane) and 56% (allyl iodide); Table 1), which have EA_v values (5.59 eV and 5.51 eV, respectively; Table 1) similar to that for **q15** (EA_v: 5.56 eV; Table 2). The reduced reactivity of the (ground) singlet state of biradical **q15** is attributed to spin-spin coupling that reduces the radical reactivity of the (ground) singlet-state biradical compared to analogous monoradicals.[22,23] The extent of this radical reactivity reducing effect was initially proposed to be related to the magnitude of $\Delta E_{S\text{-}T}$, and this has since been found to be true in many cases.[5,7,22,23] For example, biradical **q12**, which was calculated to have a similar EA_v (5.61 eV) as biradical **q15** (5.56 eV) but substantially smaller $\Delta E_{S\text{-}T}$ (−1.1 kcal mol^{-1}), reacts somewhat faster than **q15** ($\Delta E_{S\text{-}T}$: −8.3 kcal mol^{-1}) with both cyclohexane and allyl iodide (efficiencies = 9% vs. 8% (cyclohexane), and 55% vs. 42% (allyl iodide) for **q12** and **q15**, respectively; Table 2).

There were a few exceptions, though, as some biradicals exhibited greater reactivity toward allyl iodide than the related monoradicals with a similar EA_v. For example, the 2,7-didehydroquinolinium cation (**q10**), with a $\Delta E_{S\text{-}T}$ of −2.6 kcal mol^{-1}, was expected to be less reactive toward allyl iodide than the related monoradical **q1**,[11] which has an almost identical calculated EA_v (6.30 eV) as the biradical **q10** (6.31 eV). However, biradical **q10** was found to be more reactive toward allyl iodide (total reaction efficiency = 76%) than **q1** (total reaction efficiency = 64%; Table 2). This is likely due to the existence of another relatively fast reaction pathway for the biradical, abstraction of an allyl group, which occurs at a higher rate (36% branching ratio) than for the monoradical (15% branching ratio). In fact, almost all biradicals showed a smaller branching ratio for I atom abstraction and a greater branching ratio for allyl group abstraction from allyl iodide than the relevant monoradicals. This was especially notable for those biradicals that have a radical site at C–2 (Table 2). This finding suggests that allyl iodide may coordinate with these specific biradicals by forming a hydrogen bond between the iodine atom and the proton bound to the N atom, which would hinder I atom abstraction but facilitate allyl abstraction by the adjacent radical site. A similar finding was made for the related monoradicals: the monoradical that most efficiently abstracts an

allyl group is the only one (**q1**) with the radical site next to the protonated nitrogen atom (Table 1). It should also be noted here that allyl abstraction involves addition of a (bi)radical to the C=C double bond in allyl iodide, which is a fundamentally different reaction from I atom abstraction. It is possible that spin-spin coupling in biradicals hinders this reaction less than atom abstraction reactions. We are exploring this issue further.

In order to examine the efficiencies of *specific reactions* (i.e., H atom and I atom abstractions), the H and I atom abstraction efficiencies (total efficiency × branching ratio of atom abstraction) for cyclohexane and allyl iodide were plotted as a function of the (calculated) EA_v for a series of (iso)quinolinium-based mono- and biradicals (Figures 1 and 2; note that only those biradicals that underwent major I atom abstraction were included in the I atom abstraction plot).[11,14] The monoradicals showed a linear correlation for both reactions (Figures 1 and 2; note that corresponding plots of the natural logarithm of the H or I atom abstraction efficiency versus EA_v (data not shown) gave fits almost as good). While a correlation between the natural logarithm of H atom abstraction efficiency and EA_v for related monoradicals has been published previously,[9] no correlations have been reported for I atom abstraction reactions of radicals similar to those described here.

Finally, it is noteworthy that all of the (iso)quinolinium-based biradicals lie *below* the trend lines fit for the monoradicals (Figures 1 and 2). Based on the fact that the calculated EA_v values of all the biradicals are higher than those for the corresponding monoradicals, the biradicals might be expected to be more reactive than the monoradicals. However, it appears that spin-spin coupling between the two radical sites may be responsible for the lower observed reactivity of the biradicals.

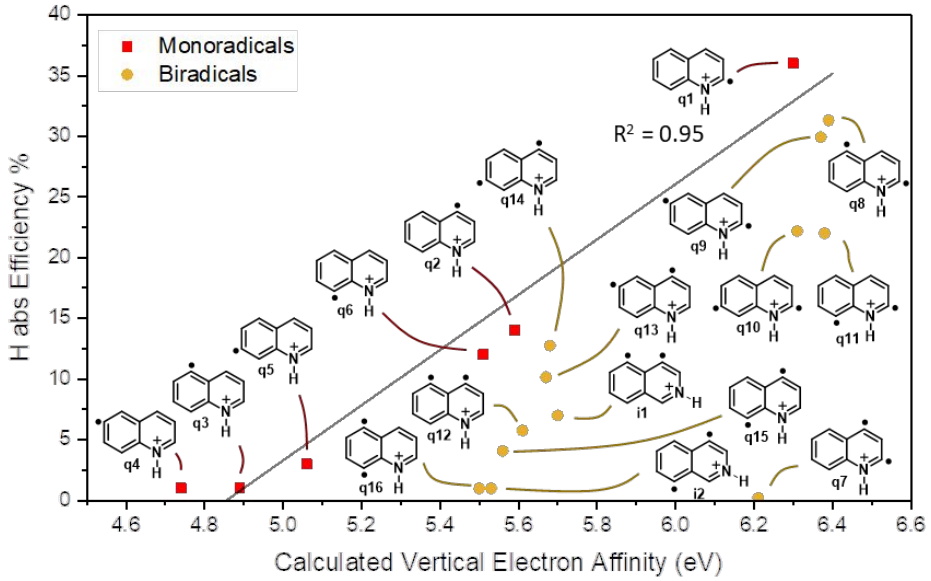

Figure 1. The efficiency of H atom abstraction from cyclohexane by (iso)quinolinium-based mono- and biradicals versus the (calculated) EA_v of the radical site(s). The data for **q1** – **q7**,[11] **i1**,[14] and **i2**[14] have been reported previously. The EA_v of **q13** and **q14** have been calculated previously.[10] The data for the monoradicals (only; red boxes) were fit to a linear trend line ($R^2 = 0.95$).

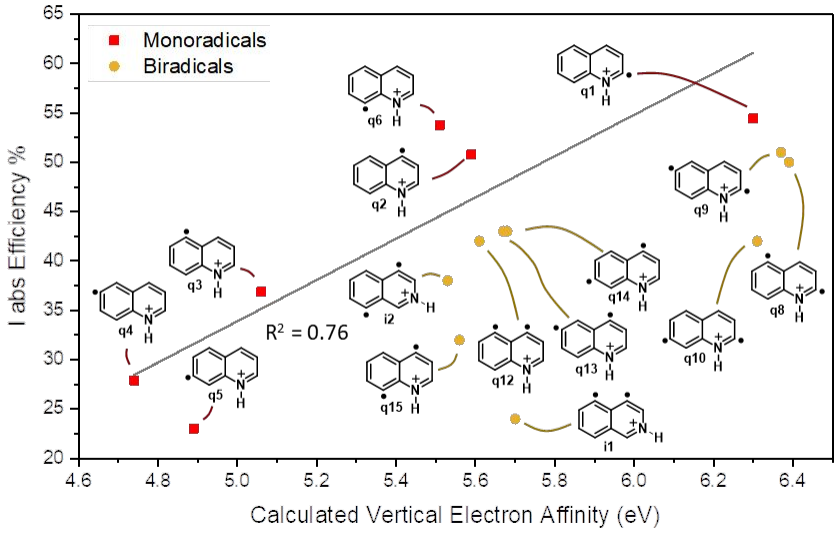

Figure 2. The efficiency of I atom abstraction from allyl iodide versus the (calculated) EA_v of the radical site(s) for those (iso)quinolinium-based mono- and biradicals that underwent a major I atom abstraction. The data for **q1** – **q7**,[11] **i1**,[14] and **i2**[14] have been reported previously. The EA_v of **q13** and **q14** have been calculated previously.[10 16] The data for the monoradicals (only; red boxes) were fit to a linear trend line ($R^2 = 0.76$).

Acridinium-based radicals. Because all of the (iso)quinolinium-based biradicals showed stabilizing interactions between the two radical sites that lowered their reactivities compared to the analogous monoradicals (Figures 1 and 2), several acridinium-based mono- and biradicals (**a1**–**a8**) were studied as they allow greater distances between the radical sites and, therefore, should have little to no spin-spin coupling (Table 3). Just like the quinolinium-based monoradicals, the acridinium-based monoradicals **a1**–**a4** exclusively undergo H atom abstraction from cyclohexane and predominant I atom abstraction from allyl iodide. Also like the quinolinium-based monoradicals, the H and I atom abstraction efficiencies measured for the acridinium-based monoradicals were found to be linearly correlated with their (calculated) EA_v (Figures 3 and 4).

Surprisingly, however, the reactivities of monoradicals **a1**–**a4** (Table 3) were found generally to be slightly *lower* than those for the related quinolinium-based monoradicals **q2**–**q5** (Table 1) despite their nearly identical EA_v. For example, the 9-dehydroacridinium cation (**a1**; EA_v: 5.63 eV) reacts with cyclohexane and allyl iodide at efficiencies of 4% and 40%, respectively, while the related quinolinium-based monoradical, the 4-dehydroquinolinium cation (**q2**; EA_v: 5.59 eV), showed total reaction efficiencies of 14% toward cyclohexane and 54% toward allyl iodide. The reasons for this behavior are not obvious.

The acridinium-based biradicals **a5**–**a8** predominantly underwent either one or two H atom abstractions as the primary reactions with cyclohexane and predominant I atom abstraction with allyl iodide (followed by a second I atom abstraction from another allyl iodide molecule; Table 3). The abstraction of two H atoms from cyclohexane and two I atoms from allyl iodide confirmed the presence of two radical sites for each biradical.

Table 3. Total Reaction Efficiencies[a] and Observed Reactions[b] With Branching Ratios,[c] and H Atom and I Atom Abstraction Efficiencies[d] for Acridinium-Based Mono- and Biradicals Upon Interaction With Cyclohexane and Allyl Iodide, and Calculated[e] Vertical Electron Affinities (EA_v) and Singlet-Triplet splittings (ΔE_{S-T})

Monoradicals	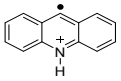 **a1**	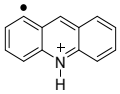 **a2**	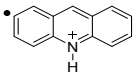 **a3**	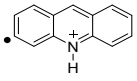 **a4**
EA_v (eV)	5.63	5.06	4.74	4.90
Cyclohexane	H abs 100% **Efficiency = 4%**	H abs 100% **Efficiency = 0.8%**	H abs 100% **Efficiency = 0.3%**	H abs 100% **Efficiency = 0.4%**
Allyl Iodide	I abs 97% Allyl abs 3% **Efficiency = 40%** **I abs eff. = 39%**	I abs 98% Allyl abs 2% **Efficiency = 33%** **I abs eff. = 32%**	I abs 94% Allyl abs 6% **Efficiency = 27%** **I abs eff. = 25%**	I abs 93% Allyl abs 7% **Efficiency = 29%** **I abs eff. = 27%**
Biradicals	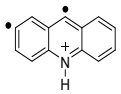 **a5**	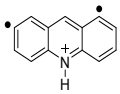 **a6**	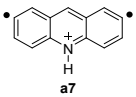 **a7**	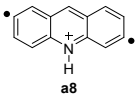 **a8**
EA_v (eV)	5.76	5.18	5.07	5.05
ΔE_{S-T} (kcal mol^{-1})	−0.6	−0.1	0.0	+0.1
Cyclohexane	H abs 72% 2 x H abs 20% Adduct 8% **Efficiency = 9%** **H abs eff. = 7%** URI[f] = 71%	H abs 62% 2 x H abs 32% Adduct 6% **Efficiency = 3%** **H abs eff. = 1.9%** URI = 48%	H abs 79% 2 x H abs 18% Adduct 3% **Efficiency = 2%** **H abs eff. = 1.6%** URI = 37%	H abs 78% 2 x H abs 16% Adduct 5% **Efficiency = 2%** **H eff. = 1.6%** URI = 45%
Allyl Iodide	I abs 81% 2° I abs Allyl abs 19% 2° I abs **Efficiency = 43%** **I abs eff. = 35%** URI = 75%	I abs 78% 2° I abs Allyl abs 22% 2° I abs **Efficiency = 35%,** **I abs eff = 27%** URI = 16%	I abs 79% 2° I abs Allyl abs 21% 2° I abs **Efficiency = 37%** **I abs eff. = 29%** URI = 11%	I abs 82% 2° I abs Allyl abs 18% 2° I abs **Efficiency = 34%** **I abs eff. = 28%** URI = 16%

[a]Percentage of collisions that lead to reaction; k_{exp}/k_{coll} (reaction rate constant / calculated collision rate constant) × 100. [b]abs = abstraction. 2° H (or I or allyl) abs implies that this H abs is a secondary reaction of the product shown just above. The identity of the primary product that produced each secondary product was deduced from the rate plots prepared for all studied reactions. When not clear, each primary product ion was isolated and its reactions examined. [c]Branching ratios of primary reactions were determined by dividing the abundance of the product ion by the sum of the abundances of all product ions. [d]H and I atom abstraction efficiencies calculated by multiplying the total reaction efficiency with the branching ratio of H atom abstraction from cyclohexane or I atom abstraction from allyl iodide. [e]EA_v values calculated at the UB3LYP/aug-cc-pVTZ//UB3LYP/cc-pVTZ level of theory; ΔE_{S-T} values calculated at the UB3LYP/cc-pVTZ//UB3LYP/cc-pVTZ level of theory. [f]URI = unreactive isomer; the structures of the unreactive isomers are unknown in most cases; the percentage of URI was determined from rate plots.

Benzannelation of the quinolinium-based biradical **q13** to give the acridinium-based biradical, **a5** (the only acridinium-based biradical studied where the positioning of the two radical sites is analogous to any of the (iso)quinolinium-based biradicals), resulted in a slight decrease in the magnitude of the singlet-triplet splitting (**q13** and **a5** have calculated ΔE_{S-T} values of –1.1 and –0.6 kcal mol^{-1}, respectively; Tables 2 and 3), a slight increase in (calculated) EA_v (5.67 and 5.76 eV, respectively), and a slight decrease in the total reaction efficiencies (cyclohexane = 13% and 9%, respectively; allyl iodide = 53% and 43%, respectively). However, the three acridinium-based

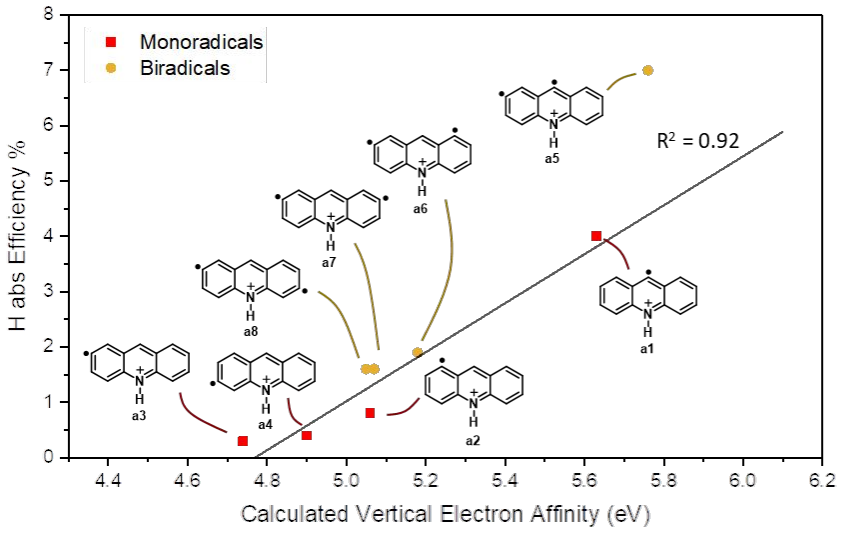

Figure 3. The efficiency of H atom abstraction from cyclohexane by acridinium-based mono- and biradicals versus the (calculated) EA_v of the radical site(s). The data for the monoradicals (only; red boxes) were fit to a linear trend line ($R^2 = 0.92$).

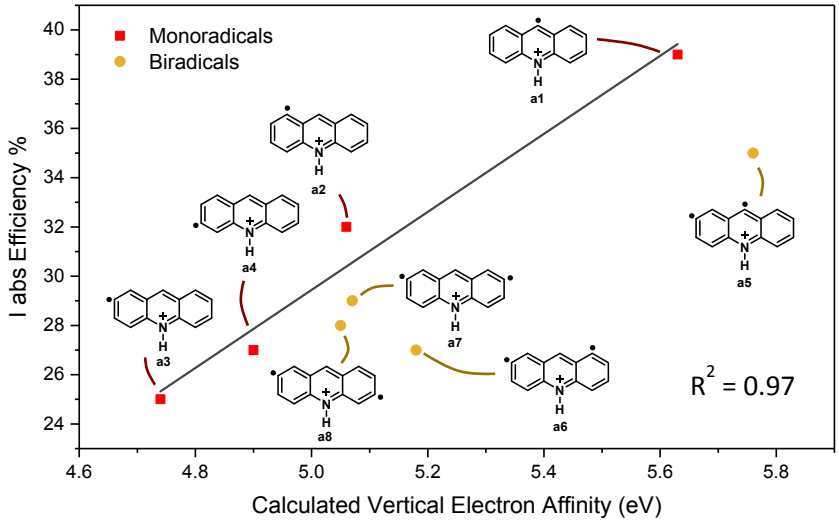

Figure 4. The efficiency of I atom abstraction from allyl iodide by acridinium-based mono- and biradicals versus the (calculated) EA_v of the radical site(s). The data for the monoradicals (only; red boxes) were fit to a linear trend line ($R^2 = 0.97$).

biradicals with greater separations between their radical sites have smaller $\Delta E_{S\text{-}T}$ (ranging from –0.1 to +0.1 kcal mol^{-1}; Table 3), smaller EA_v (5.05–5.18 eV) and lower reactivity (for cyclohexane, 2–3% total reaction efficiency) than 10 of the 12 (iso)quinolinium-based biradicals studied. The smaller $\Delta E_{S\text{-}T}$ and EA_v values are due to a greater distance between the radical sites, and between the radical sites and the protonated nitrogen atom, respectively. For biradicals **a6**–**a8**, therefore, it appears that the lowering of EA_v is primarily responsible for their lower reactivity (i.e., compared to the (iso)quinolinium-based biradicals) since lowering of $\Delta E_{S\text{-}T}$ (less spin–spin coupling) would be expected to lead to higher reactivity.

As the number of carbon-carbon bonds between the two radical sites increases in the

acridinium-based biradicals from **a5** to **a8** (3, 5, 6 and 7 bonds, respectively), the calculated ΔE_{S-T} was found to systematically become more positive (−0.6, –0.1, 0.0 and +0.1 kcal mol^{-1}, respectively; Table 3). Such a correlation does not exist for the (iso)quinolinium-based biradicals, which is likely due to the very different nonbonding orbital orientations in these systems, which strongly influence[4-6] spin–spin coupling. It is also noteworthy that the orientation of the nonbonding orbitals in biradical **a7** might, in fact, be expected to lead to relatively weak through-bond spin-spin coupling (via a "W"-type arrangement like that in **q10**); however, the calculated ΔE_{S-T} (0.0 kcal mol^{-1}) suggests that the distance between the two radical sites is too large for any significant spin-spin interaction (at least at the DFT level of theory used here to calculate ΔE_{S-T}). Thus, based on the ΔE_{S-T} values, most of the acridinium-based biradicals should behave like they contain two isolated radical sites, which should result in equal or greater reactivity than for the monoradicals with a similar EA_v. Indeed, the total reaction efficiencies of **a7** and **a8** for cyclohexane (both 2%; Table 3) are greater than that of monoradical **a2** (efficiency 0.8%) with a similar EA_v (5.06 eV) as **a7** and **a8** (5.07 and 5.05 eV, respectively). Total reaction efficiencies for allyl iodide are similar or slightly greater than that of the monoradical **a2** (**a7**, **a8** and **a2**: total reaction efficiencies are 37%, 34% and 33%, respectively). On the other hand, although the magnitude of ΔE_{S-T} for biradical **a5** is calculated to be the largest among the acridinium-based biradicals (–0.6 kcal mol^{-1}), it showed the highest reactivity toward both cyclohexane and allyl iodide (Table 3). This can be attributed to its relatively high EA_v (5.76 eV; EA_v of the other biradicals range from 5.05 eV to 5.18 eV).

In order to examine the efficiencies of *specific reactions*, the efficiency of H atom abstraction from cyclohexane was plotted as a function of the (calculated) EA_v for all the acridinium-based mono- and biradicals (Figure 3). In this plot, the data for the biradicals (**a5**–**a8**) lie above the monoradical trend line (Figure 3) as opposed to below it as observed for the related (iso)quinolinium-based biradicals (Figure 1). This suggests somewhat greater reactivities for the acridinium-based biradicals than the related monoradicals, which is likely due to the very weak, to absent, spin-spin coupling between the radical sites in **a5**–**a8**. Therefore, when the radical sites are located on benzene rings that are not adjacent to each other, they do not appear to interact. A different result was obtained for I atom abstraction from allyl iodide. In the plot (Figure 4), the data for the acridinium-based biradicals lie *below* the monoradical trend line. The reasons for this difference are not known at this time.

Identification of the most reactive radical site in the biradicals. Among all the previously reported biradicals of the type discussed here, the radical site that reacts *first* has only been experimentally identified for one biradical, the 4,5-didehydroisoquinolinium cation (**i1**), that first abstracts a H atom from cyclohexane at the radical site C−4.[8] In order to identify the radical site that reacts first for the other studied biradicals, the products of the quinolinium-based biradicals **q7** – **q16** formed upon abstraction of a H atom from cyclohexane (MS/MS experiments) were isolated in the ion trap and allowed to undergo further reactions for 300 ms with cyclohexane (MS/MS/MS experiments). The MS/MS/MS spectra were compared with MS/MS spectra measured for authentic, isomeric monoradicals collected on the same instrument on the same day (Figure 5) in order to identify the structures of the unknown monoradicals. For all biradicals containing a radical site at C−2 (**q7** - **q11**), this site was found to react first as none of the unknown monoradical products showed the same relative abundances of ions m/z 129 and m/z 130 as authentic 2-dehydroquinolinium cation (**q1**). Moreover, each of the MS/MS/MS spectra measured for the

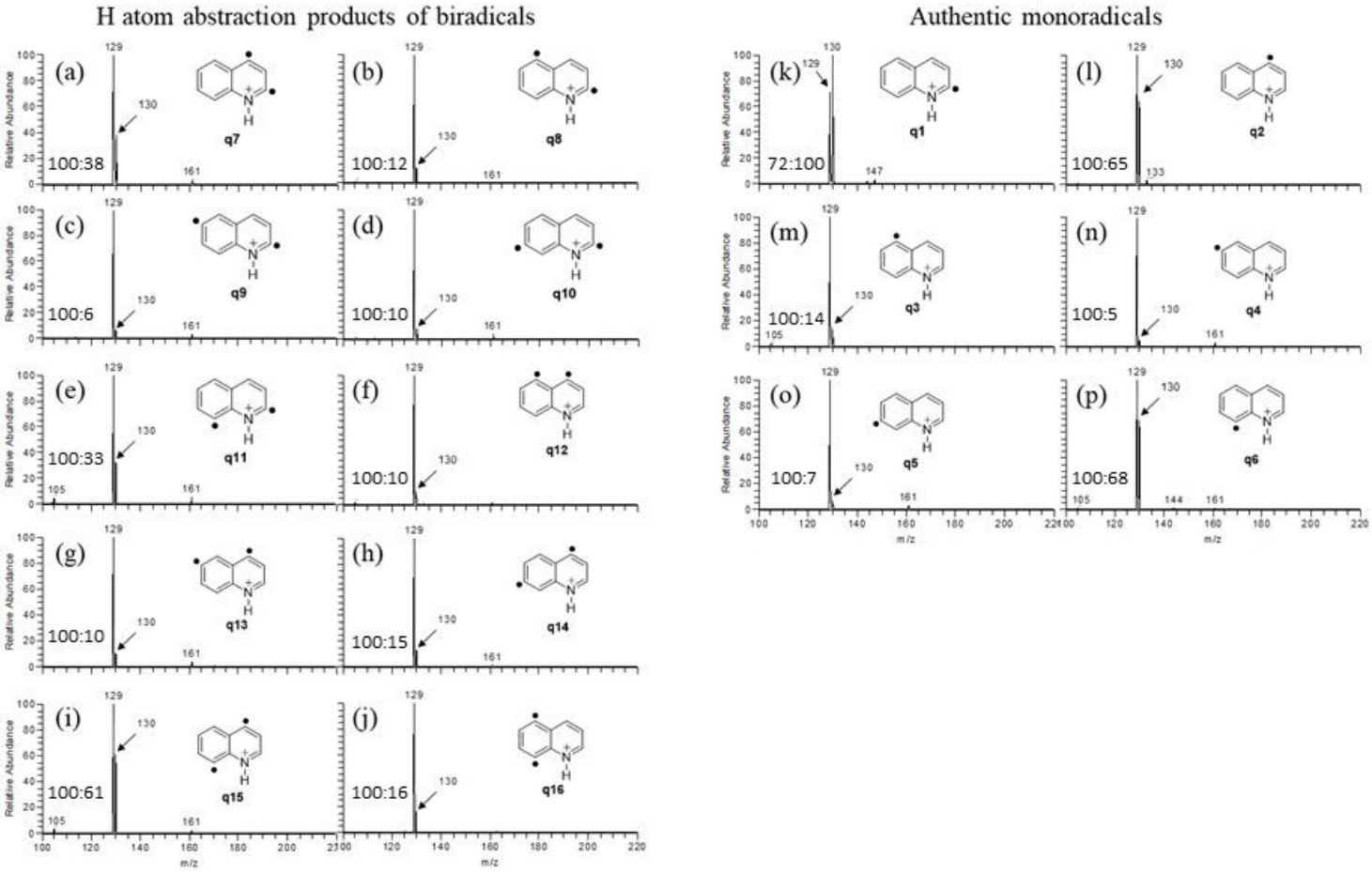

Figure 5. (a–j) MS/MS/MS spectra measured after 300 ms reaction with cyclohexane for the isolated H abstraction products (m/z 129) of quinolinium-based biradicals, **q7**–**q16**; (k–p) MS/MS spectra measured after 300 ms reaction with cyclohexane for the isolated, authentic monoradicals, **q1**–**q6**. The major product is the H atom abstraction product (m/z 130). The ions of m/z 161, 147, 133, and 105 are assigned as background oxygen adduct, background water adduct, oxygen adduct that has lost CO, and oxygen adduct that has lost two molecules of CO, respectively. In this case, then, both of the C−4 and C−8 radical sites in **q15** may undergo the first H atom abstraction. In summary, the radical site that reacts first for each biradical is the one predicted to be more reactive based on the reactivities of the authentic monoradicals (whose reactivities correlate with their EA_v). The ratios of the peaks m/z 129 and m/z 130 are provided in the bottom left part of each mass spectrum.

unknown monoradicals was similar to the MS/MS spectrum measured for the expected authentic monoradical, thus confirming that the radical site at C−2 reacted first and that the resulting monoradical had the expected structure (e.g., the MS/MS/MS spectrum measured for the monoradical reaction product of **q7** (with radical sites at C−2 and C−4) is similar to that measured for **q2 (**C−4 radical site)). For **q16** (with radical sites at C−5 and C−8), the radical site at C−8 is more reactive, again as expected based on the monoradical reactivities (Table 1).

Similarly, the biradicals with a radical site at C−4 (**q12**–**q14)** reacted first at the C−4 radical site with cyclohexane (Figure 5). These results are consistent with the results previously reported

for the 4,5-didehydroisoquinolinium cation (**i1**; see above). However, the 4- and 8-dehydroquinolinium cations (**q2** and **q6**) have very similar reactivity toward cyclohexane (and allyl iodide; Table 1). The MS/MS/MS spectrum measured for the H atom abstraction product of the 4,8-didehydroquinolinium cation (**q15**, Figure 5i) resembles both of those measured for **q2** and **q6**.

The radical site that reacts first for the acridinium-based biradical, **a5**, was identified experimentally as described above for the quinolinium-based biradicals. As shown in Figure 6, the H atom abstraction product of **a5** formed upon reaction with cyclohexane showed relatively low reactivity, which is similar to the behavior of the related monoradical, **a3**. This result indicates that the first H abstraction occurs at the radical site at C−9 of **a5**, which is consistent with the observations described above for the quinolinium-based systems for which the radical site predicted to be more reactive based on related monoradical reactivities reacts first. Unfortunately, similar experiments for biradicals **a6**–**a8** were inconclusive because the related monoradicals **a2**–**a4** display similar and low reactivity toward cyclohexane.

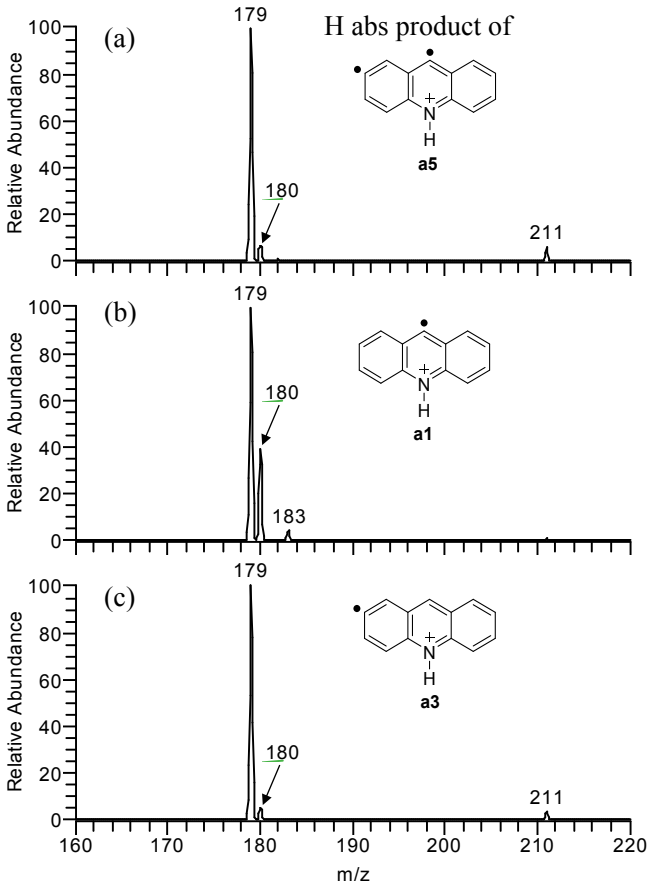

Figure 6. (a) MS/MS/MS spectrum measured after 500 ms reaction with cyclohexane for the H atom abstraction product of **a5** (m/z 179); (b, c) MS/MS spectra measured for the authentic monoradicals **a1** and **a3**, respectively. The product ions arise from H atom abstraction (m/z 180), background oxygen addition (m/z 211) and background oxygen addition followed by elimination of carbon monoxide (m/z 183). Note that the virtually identical spectra, (a) and (c), indicate that the H atom abstraction product of **a5** is **a3**.

CONCLUSIONS

A linear correlation was identified for all studied monoradicals for the H atom and I atom abstraction efficiencies from cyclohexane and allyl iodide, respectively, as a function of the (calculated) EA_v of the monoradicals. As opposed to H atom abstraction efficiency, I atom abstraction efficiency has not been previously correlated with any reactivity-controlling factor for related radical systems. The acridinium-based monoradicals were found to be slightly less reactive than the related (iso)quinolinium-based monoradicals in spite of similar EA_v values.

The reactivities of the (iso)quinolinium-based biradicals were found not to correlate individually with either their ΔE_{S-T} or EA_v values, as they are likely to depend on both and possibly also on other yet unidentified variables. However, plots of the efficiencies of H and I atom abstraction from cyclohexane and allyl iodide, respectively, as a function of the (calculated) EA_v for the various (iso)quinolinium-based mono- and biradicals showed that all of the biradicals lie below the trend line for the monoradicals, hence showing lower reactivity than the monoradicals.

In sharp contrast, the acridinium-based biradicals displayed slightly greater reactivity toward cyclohexane than the related monoradicals. Therefore, when the two radical sites in these biradicals are farther apart than in the same or in two adjacent aromatic rings (with one exception), the radical sites appear not to interact and, as a result, no suppression of radical reactivity was observed. Indeed, based on the (very small) calculated ΔE_{S-T} values, most of the acridinium-based biradicals should behave like they contain two individual monoradicals. Moreover, a plot of the efficiencies of H atom abstraction from cyclohexane as a function of the (calculated) EA_v for the acridinium-based mono- and biradicals revealed slightly greater reactivity for the biradicals. However, the acridinium-based biradicals did not show greater reactivity than the relevant monoradicals in I atom abstraction reactions, possibly due to competing reactions that were not accounted for.

Most of the acridinium-based biradicals have greater separations between their radical sites than the (iso)quinolinium-based biradicals, and they all have smaller ΔE_{S-T} and smaller EA_v values due to the greater distance between the radical sites, and between both radical sites and the protonated nitrogen atom. The reduction of both of these reactivity-controlling factors explains the generally lower total reaction efficiencies compared to the (iso)quinolinium-based biradicals.

For each biradical examined, the radical site that reacts first was found to be the same site that is predicted to be more reactive based on the reactivities of authentic monoradicals. Because the reactivity of the monoradicals reflects their (calculated) EA_v values, calculation of the EA_v values for the relevant monoradicals enables the prediction of the more reactive radical site in such biradicals.

EXPERIMENTAL SECTION

Quinolinium-based monoradicals **q1**–**q6**, biradical **q7**, and isoquinolinium-based biradicals **i1** and **i2** have been studied previously.[11,14] The precursors (Chart 3) for quinolinium-based radicals **q1**–**q9**, **q12–q14**, and **q16** were synthesized as described in the literature.[10,24] Precursors for quinolinium-based biradicals **q10**, **q11** and **q15** and acridinium-based monoradicals **a1**–**a8** were synthesized as described below. All other chemicals were purchased from Sigma-Aldrich and used without further purification.

The reactivity and kinetic studies were performed using a previously reported approach.[10,11]

Briefly, radical precursors were protonated using an atmospheric pressure chemical ionization (APCI) source of a linear quadrupole ion trap (LQIT) mass spectrometer coupled with a reagent inlet manifold described previously.[25] The ions were transferred into the ion trap. The desired ions were isolated by ejecting all the unwanted ions from the trap. Collision-activated dissociation (CAD) was used to cleave off iodine atom(s) and/or a nitro group from the protonated (bi)radical precursors to generate the desired radical site(s). The protonated radicals were isolated and allowed to react with the neutral reagent for a variable period of time before all ions were ejected from the ion trap and detected. The reagent was injected into the heated manifold at a flow rate of 5 μL h^{-1}. The evaporated reagent was mixed with helium buffer gas and introduced into the ion trap.[10]

Kinetic data for the reactions were collected to identify the primary and secondary reaction products and to determine second-order reaction rate constants. The measured second-order reaction rate constants (see Supporting Information) were divided by calculated collision rate constants (k_{exp}/k_{coll}; see Supporting Information) to give reaction efficiencies (i.e., the percentage of collisions leading to a reaction). The collision rate constants were calculated using a parameterized trajectory theory.[26]

Syntheses (all synthesis schemes and ^{1}H and ^{13}C NMR spectra are provided in SI)

2-Iodo-7-nitroquinoline (q10a). 2-Chloro-7-nitroquinoline (30 mg, 0.14 mmol) was dissolved in anhydrous acetonitrile. Acetyl chloride (31 mg, 0.39 mmol) and anhydrous sodium iodide (180 mg, 1.20 mmol) were added into the solution. The solution was refluxed in an oil bath for 24 h under argon. After cooling to room temperature, the solution was diluted with dichloromethane and washed with sodium carbonate and sodium sulfite, consecutively. The solvent was removed under low pressure. 3 mg of the residue was purified through a reversed phase C18 preparative HPLC column (50:50 water/acetonitrile to 5:95 water/acetonitrile) to yield a white solid product. ^{1}H NMR (800 MHz, chloroform-*d*) δ 8.98 (s, 1H), 8.37 (d, J = 8.9 Hz, 1H), 7.98 (d, J = 8.9 Hz, 1H), 7.94 (d, J = 8.5 Hz, 1H), 7.89 (d, J = 8.4 Hz, 1H). $^{13}C\{^{1}H\}$ NMR (201 MHz, $CDCl_3$) δ 148.4, 148.3, 136.5, 135.0, 130.2, 129.5, 125.0, 121.7, 120.8. HRMS (APCI), calcd. for $C_9H_6N_2O_2I$: 300.9474 $[M+H]^+$, found: 300.9451.

2-Chloro-8-nitroquinoline (s1). 1 mL of concentrated nitric acid and 4 mL of concentrated sulfuric acid were mixed, and 645 mg of 2-chloroquinoline (3.92 mmol, purchased from Sigma-Aldrich), was added. The solution was stirred under room temperature for 12 h, then poured on ice and neutralized with 33% ammonium hydroxide solution until a pH of 7. The precipitated solid was filtered and purified by silica column chromatography (5:95 ethyl acetate/hexanes) to yield 2-chloro-5-nitroquinoline (226 mg, 28%) and 2-chloro-8-nitroquinoline (378 mg, 46%) as light yellow solid. ^{1}H NMR (400 MHz, chloroform-*d*) δ 8.20 (d, J = 8.6 Hz, 1H), 8.09 (dd, J = 7.6, 1.4 Hz, 1H), 8.04 (dd, J = 8.3, 1.4 Hz, 1H), 7.64 (dd, J = 8.2, 7.6 Hz, 1H), 7.54 (d, J = 8.6 Hz, 1H). The ^{1}H NMR is consistent with literature.[27]

8-Amino-2-chloroquinoline (s2). 2-Chloro-8-nitroquinoline (300 mg, 1.44 mmol) and iron powder (252 mg, 4.46 mmol) were mixed in 4.5 mL of methanol and cooled to 0 °C. While stirring, 1.5 mL of concentrated hydrochloric acid was added dropwise. The solution was allowed to warm to room temperature and stirred for 5 min, then neutralized with sodium carbonate until pH of 9.

The mixture was extracted with dichloromethane (three times, 20 mL each) and dried with anhydrous sodium sulfate. A silica column pretreated with 1% triethylamine hexanes solution was used to purify the product (1:9 ethyl acetate/hexanes). The product was a yellow solid (143 mg, 56%). ^{1}H NMR (400 MHz, chloroform-*d*) δ 8.00 (d, *J* = 8.6 Hz, 1H), 7.36 – 7.31 (m, 2H), 7.13 (dd, *J* = 8.1, 1.3 Hz, 1H), 6.94 (dd, *J* = 7.6, 1.3 Hz, 1H), 4.88 (s, 2H). ^{13}C{^{1}H} NMR (101 MHz, $CDCl_3$) δ 147.9, 143.1, 138.9, 137.6, 127.7, 127.4, 122.3, 115.6, 111.2. HRMS (APCI), calcd. for $C_9H_8N_2Cl$: 179.0376 $[M+H]^+$, found: 179.0361, 181.0332.

2-Chloro-8-iodoquinoline (s3). 8-Amino-2-chloroquinoline (129 mg, 0.72 mmol) was dissolved in a mixture of 3 N hydrochloric acid (5 mL) and methanol (5 mL) and cooled to 0 °C. Into this solution, 1.3 mL of sodium nitrite solution (172 mg, 2.50 mmol) was slowly added. The reaction was stirred at 0 °C for 10 min. 174 mg of copper(I) iodide dispersed in 2.2 mL of water was added into the solution, followed by addition of 1.1 mL of 57% hydroiodic acid. After 5 min, the reaction mixture was poured onto ice and neutralized with sodium carbonate. The solution was extracted by dichloromethane (three times, 20 mL each) and dried with anhydrous sodium sulfate. A silica column pretreated with 1% triethylamine hexanes solution was used to purify the product (1:9 ethyl acetate/hexanes). The product was a pale white solid (80 mg, 40%). ^{1}H NMR (400 MHz, chloroform-*d*) δ 8.33 (dd, *J* = 7.4, 1.3 Hz, 1H), 8.04 (d, *J* = 8.5 Hz, 1H), 7.79 (dd, *J* = 8.1, 1.3 Hz, 1H), 7.40 (d, *J* = 8.5 Hz, 1H), 7.27 (dd, *J* = 8.1, 7.4 Hz, 1H). ^{13}C{^{1}H} NMR (101 MHz, $CDCl_3$) δ 151.9, 147.1, 141.0, 139.4, 128.3, 128.0, 127.3, 123.4, 101.4. HRMS (APCI), calcd. for C_9H_6NICl: 289.9234 $[M+H]^+$, found: 289.9211, 291.9186.

2,8-Diiodoquinoline (q11a). 2-Chloro-8-iodoquinoline (80 mg, 0.28 mmol), anhydrous sodium iodide (428 mg, 2.85 mmol) and copper(I) iodide (5 mg, 0.026 mmol) were charged in a Schlenk tube. The tube was subjected to vacuum and refilled with argon three times. 0.6 mL of 1,4-dioxane containing 8 mg of N,N'-dimethyl-1,2-cyclohexanediamine (0.056 mmol) was added into the Schlenk tube and sealed. The solution was stirred in an oil bath at 110 °C. After three days, the solution was cooled to room temperature, quenched with 1 mL of 33% ammonium hydroxide and extracted with dichloromethane (three times, 2 mL each). The solution was dried with anhydrous sodium sulfate and purified using a silica column pretreated with 1% triethylamine hexanes solution (1:9 ethyl acetate/hexanes). The product was then recrystallized in a mixture of dichloromethane and hexanes, yielding as white solid (16 mg, 15%). ^{1}H NMR (400 MHz, chloroform-*d*) δ 8.32 (dd, *J* = 7.4, 1.2 Hz, 1H), 7.77 – 7.73 (m, 2H), 7.67 (d, *J* = 8.4 Hz, 1H), 7.29 – 7.24 (m, 1H). ^{13}C{^{1}H} NMR (101 MHz, $CDCl_3$) δ 148.6, 140.5, 137.3, 133.1, 128.6, 128.1, 127.6, 120.1, 102.1. HRMS (APCI), calcd. for $C_9H_6NI_2$: 381.8590 $[M+H]^+$, found: 381.8567.

4-Chloro-8-nitroquinoline (s4). 3 mL of concentrated nitric acid and 12 mL of concentrated sulfuric acid were mixed, and 1.00 g of 4-chloroquinoline (6.11 mmol, purchased from Sigma-Aldrich), was added. The solution was stirred under room temperature for 1 h, then poured onto ice and neutralized with 33% ammonium hydroxide solution until at pH of 7. The precipitated solid was filtered and purified by flash column chromatography (1:9 ethyl acetate/hexanes) to yield 4-chloro-5-nitroquinoline (216 mg, 17%) and 4-chloro-8-nitroquinoline (774 mg, 61%) as white solids. ^{1}H NMR (400 MHz, chloroform-*d*) δ 8.93 (d, *J* = 4.7 Hz, 1H), 8.47 (dd, *J* = 8.5, 1.4 Hz, 1H),

8.07 (dd, J = 7.5, 1.4 Hz, 1H), 7.73 (dd, J = 8.6, 7.5 Hz, 1H), 7.65 (d, J = 4.7 Hz, 1H). The ^{1}H NMR is consistent with literature.[28]

8-Amino-4-chloroquinoline (s5). 4-Chloro-8-nitroquinoline (270 mg, 1.29 mmol) and iron powder (217 mg, 3.84 mmol) were mixed in 4 mL of methanol and cooled to 0 °C. While stirring, 1.5 mL of concentrated hydrochloric acid was added dropwise. The solution was allowed to warm to room temperature and stirred for 1 h, then neutralized with sodium carbonate until at pH of 9. The mixture was extracted with dichloromethane (three times, 20 mL each) and dried with anhydrous sodium sulfate. A silica column pretreated with 1% triethylamine hexanes solution was used to purify the product (1:9 ethyl acetate/hexanes). The product was a yellow solid (212 mg, 92%). ^{1}H NMR (400 MHz, chloroform-*d*) δ 8.60 (d, J = 4.6 Hz, 1H), 7.52 (dd, J = 8.4, 1.3 Hz, 1H), 7.46 (d, J = 4.6 Hz, 1H), 7.41 (dd, J = 8.4, 7.5 Hz, 1H), 6.97 (dd, J = 7.5, 1.3 Hz, 1H), 5.03 (s, 2H).[36] ^{13}C{^{1}H} NMR (101 MHz, $CDCl_3$) δ 146.4, 144.2, 142.4, 139.0, 128.3, 127.0, 121.5, 112.1, 110.7. HRMS (APCI), calcd. for $C_9H_8N_2Cl$: 179.0376 $[M+H]^+$, found: 179.0365, 181.0337.

4-Chloro-8-iodoquinoline (s6). 8-Amino-2-chloroquinoline (212 mg, 1.19 mmol) was dissolved in 5 mL of 3 N hydrochloric acid and cooled to 0 °C. Into this solution, 123 mg sodium nitrite (1.78 mmol) in 1 mL water was slowly added. The reaction was stirred at 0 °C for 10 min. 272 mg of copper(I) iodide (1.42 mmol) dispersed in 2 mL of water was added into the reaction mixture followed by addition of 1.5 mL of 57% hydroiodic acid. After 5 min, the reaction mixture was poured onto ice and neutralized with sodium carbonate. The solution was extracted by dichloromethane (three times, 20 mL each) and dried with anhydrous sodium sulfate. A silica column pretreated with 1% triethylamine hexanes solution was used to purify the product (1:9 ethyl acetate/hexanes). The product was a pale white solid (130 mg, 39%). ^{1}H NMR (800 MHz, chloroform-*d*) δ 8.91 (d, J = 4.7 Hz, 1H), 8.43 (d, J = 7.8 Hz, 1H), 8.28 (d, J = 7.8 Hz, 1H), 7.59 (d, J = 4.7 Hz, 1H), 7.38 (t, J = 7.8 Hz, 1H). ^{13}C{^{1}H} NMR (201 MHz, $CDCl_3$) δ 150.6, 147.9, 143.0, 141.2, 128.7, 127.0, 125.2, 122.0, 103.6. HRMS (APCI), calcd. for C_9H_6NICl: 289.9234 $[M+H]^+$, found: 289.9210, 291.9183.

4,8-Diiodoquinoline (q15a). 4-Chloro-8-iodoquinoline (100 mg, 0.36 mmol) was dissolved in anhydrous acetonitrile. Acetyl chloride (84 mg, 1.13 mmol) and anhydrous sodium iodide (535 mg, 3.57 mmol) were added into the solution. The solution was refluxed in an oil bath for 24 h under argon. After cooling to room temperature, the solution was diluted with dichloromethane and washed with sodium carbonate and sodium sulfite consecutively. The solvent was removed under low pressure. The residue was purified with a silica flash column (1:9 ethyl acetate/hexanes) to give a white solid product (106 mg, 77%). ^{1}H NMR (400 MHz, chloroform-*d*) δ 8.54 (d, J = 4.5 Hz, 1H), 8.38 (dd, J = 7.4, 1.3 Hz, 1H), 8.07 – 8.00 (m, 2H), 7.33 (dd, J = 8.4, 7.4 Hz, 1H). ^{13}C{^{1}H} NMR (101 MHz, $CDCl_3$) δ 150.5, 146.6, 141.1, 133.5, 133.0, 130.6, 129.0, 112.0, 103.6. HRMS (APCI), calcd. for $C_9H_6NI_2$: 381.8590 $[M+H]^+$, found: 381.8572.

General procedure to synthesize mono- and diiodoacridines. Most of the substituted acridines were obtained by reduction of synthesized 9(10*H*)-acridone derivatives. Substituted acridone (0.24 mmol) was mixed with anhydrous tetrahydrofuran (THF, 2 mL) and borane-THF solution (1M, 0.27 mL) in a Schlenk tube under argon. The mixture was heated in an oil bath to

100°C and stirred for 1 h. After cooling to room temperature, the mixture was poured into an iron(III) chloride solution (121 mg anhydrous in 10 mL ethanol and 2 mL water) and stirred in an oil bath at 50°C for 30 min. The reaction was quenched with saturated sodium bicarbonate solution and extracted with dichloromethane (three times, 20 mL each). The solution was dried with anhydrous sodium sulfate and concentrated under reduced pressure. The residue was purified using silica column chromatography (5% ethyl acetate in hexanes).

2-((3-Iodophenyl)amino)benzoic acid (s7). 2-Chlorobenzoic acid (2.34 g, 15.0 mmol) and 3-iodoaniline (3.27 g, 14.9 mmol), potassium carbonate (2.05 g, 14.9 mmol), copper(II) sulfate (15 mg, 0.094 mmol), copper(I) iodide (45 mg, 0.24 mmol), copper powder (42 mg, 0.66 mmol) and water (15 mL) were mixed in a round bottom flask and stirred in an oil bath at 100°C for 12 h. The black solution was filtered hot and washed with 20 mL of water. The filtrate was neutralized with excess of acetic acid, during which light grey solid precipitated. The solid was collected after another filtration (1.12 g, yield 22%). (+)APCI-MS: m/z: 340 $[M+H]^+$. ^{1}H NMR (800 MHz, Methanol-d_4) δ 8.01 (dd, J = 8.0, 1.7 Hz, 1H), 7.59 (t, J = 1.9 Hz, 1H), 7.42 – 7.38 (m, 2H), 7.28 (dd, J = 8.5, 1.1 Hz, 1H), 7.24 (ddd, J = 8.1, 2.2, 0.9 Hz, 1H), 7.10 (t, J = 7.9 Hz, 1H), 6.83 (ddd, J = 8.1, 7.0, 1.1 Hz, 1H). ^{13}C{^{1}H} NMR (201 MHz, CD_3OD_SPE) δ 170.3, 146.6, 142.7, 133.7, 132.0, 131.5, 130.6, 129.4, 120.0, 117.8, 114.0, 113.3, 93.8.

1- and 3-iodoacridones (s8 and **s9)**. 2-((3-Iodophenyl)amino)benzoic acid (501 mg, 1.48 mmol) was dissolved in concentrated sulfuric acid (6 mL) and stirred in an oil bath at 100°C for 3 h. The solution was poured on 30 g ice and a greenish grey solid precipitated. The solid was filtered and washed with massive amounts of water, followed by 5 mL 0.2% ammonium hydroxide solution. The solid was vacuum dried and used without further purification.

1- and 3-iodoacridines (a2a and **a4a)**. The product from the above step was used as described in the general procedure. 1-Iodoacridine (16 mg, yield 3.5%) and 3-iodoacridine (11 mg, yield 2.4%) were collected as pale yellow solid.

1-iodoacridine. ^{1}H NMR (800 MHz, Chloroform-*d*) δ 8.99 (s, 1H), 8.27 (d, J = 8.7 Hz, 1H), 8.24 (d, J = 8.7 Hz, 1H), 8.15 (d, J = 7.0 Hz, 1H), 8.11 (d, J = 8.3 Hz, 1H), 7.85 (dd, J = 8.4, 6.6 Hz, 1H), 7.61 (dd, J = 8.7, 6.6 Hz, 1H), 7.49 (dd, J = 8.7, 7.0 Hz, 1H). ^{13}C{^{1}H} NMR (201 MHz, $CDCl_3$) δ 149.6, 148.8, 141.1, 137.0, 131.1, 130.9, 130.6, 129.0, 128.4, 128.1, 127.5, 126.4, 98.7. HRMS (APCI), calcd. for $C_{13}H_9NI$: 305.9780 $[M+H]^+$, found: 305.9757.

3-Iodoacridine. ^{1}H NMR (800 MHz, Chloroform-*d*) δ 8.76 – 8.73 (m, 2H), 8.23 (d, J = 8.7 Hz, 1H), 8.00 (d, J = 8.3 Hz, 1H), 7.83 (t, J = 7.7 Hz, 1H), 7.78 (d, J = 8.8 Hz, 1H), 7.73 (dd, J = 8.7, 2.2 Hz, 1H), 7.59 (t, J = 7.6 Hz, 1H). ^{13}C{^{1}H} NMR (201 MHz, $CDCl_3$) δ 149.3, 149.3, 138.6, 136.3, 134.3, 131.0, 129.5, 129.1, 128.3, 126.8, 126.2, 125.3, 97.1. HRMS (APCI), calcd. for $C_{13}H_9NI$: 305.9780 $[M+H]^+$, found: 305.9752.

2-Iodoacridone (s10). Acridone (226 mg, 1.16 mmol) was dissolved in 5 mL glacier acetic acid and iodine chloride (207 mg, 1.28 mmol) was added dropwise. The solution was refluxed in an oil bath for 4 h and then cooled to room temperature. The product was collected through filtration as a brown solid and washed with water. The insoluble solid was used without further purification. HRMS (APCI), calcd. for $C_{13}H_9NOI$: 321.9729 $[M+H]^+$, found: 321.9708.

2-Iodoacridine (a3a). 2-Iodoacridone obtained from above synthesis was treated as described in the general procedure to give the product as an orange solid (127 mg, yield 36%). ^{1}H NMR (400 MHz, Chloroform-*d*) δ 8.65 (s, 1H), 8.42 (d, *J* = 1.4 Hz, 1H), 8.21 (d, *J* = 8.9 Hz, 1H), 8.00 (d, *J* = 8.5 Hz, 1H), 7.97 (t, *J* = 1.2 Hz, 2H), 7.84 – 7.78 (m, 1H), 7.60 – 7.53 (m, 1H). ^{13}C{^{1}H} NMR (101 MHz, $CDCl_3$) δ 149.2, 147.5, 138.6, 136.8, 134.7, 131.0, 130.7, 129.4, 128.2, 128.0, 126.6, 126.3, 91.2. HRMS (APCI), calcd. for $C_{13}H_9NI$: 305.9780 $[M+H]^+$, found: 305.9758.

9-Chloroacridine (s11). Acridone (118 mg, 0.61 mmol) was dissolved in 3 mL of phosphorus(V) oxychloride and refluxed in an oil bath for 12 h. After cooling to room temperature, the solvent was removed under reduced pressure. The residue was neutralized with cold 1M sodium hydroxide solution, during which a solid was formed. After filtration, the solid was washed with water and a small amount of methanol and then vacuum dried to yield the product as a yellow solid (73 mg, yield 56%). ^{1}H NMR (400 MHz, Chloroform-*d*) δ 8.44 (dd, *J* = 8.8, 1.4 Hz, 2H), 8.23 (dt, *J* = 8.8, 1.3 Hz, 2H), 7.82 (ddd, *J* = 8.8, 6.6, 1.4 Hz, 2H), 7.64 (ddd, *J* = 8.8, 6.6, 1.2 Hz, 2H). ^{13}C{^{1}H} NMR (101 MHz, $CDCl_3$) δ 206.9, 148.9, 130.5, 129.7, 126.8, 124.6, 124.2. HRMS (APCI), calcd. for $C_{13}H_9NCl$: 214.0424 $[M+H]^+$, found: 214.0407, 216.0383.

9-Iodoacridine (a1a). 9-Chloroacridone (73 mg, 0.34 mmol), sodium iodide (525 mg, 3.5 mmol), copper(I) iodide (14 mg, 0.073 mmol), N,N'-dimethyl-1,2-cyclohexane diamine (22 mg, 0.15 mmol) and 1,4-dioxane (1 mL) were charged into a Schlenk tube. The solution was stirred in an oil bath at 110°C for 48 h. After cooling, the reaction was quenched with 1 mL 10 wt.% ammonium hydroxide solution and extracted with dichloromethane (three times, 10 mL each). The organic layer was washed with brine and the solvent was removed under reduced pressure. After recrystallization in ethyl acetate, the product was obtained as a yellow solid (19 mg, yield 18%). ^{1}H NMR (400 MHz, Chloroform-*d*) δ 8.34 (dt, *J* = 8.8, 1.3 Hz, 2H), 8.19 (dt, *J* = 8.7, 1.2 Hz, 2H), 7.79 (ddd, *J* = 8.8, 6.6, 1.3 Hz, 2H), 7.64 (ddd, *J* = 8.9, 6.6, 1.2 Hz, 2H). ^{13}C{^{1}H} NMR (101 MHz, $CDCl_3$) δ 148.5, 132.9, 130.4, 129.8, 129.8, 127.7, 120.0. HRMS (APCI), calcd. for $C_{13}H_9NI$: 305.9780 $[M+H]^+$, found: 305.9759.

2,9-Diiodoacridine (a5a). 2-Iodoacridone (73 mg, 0.23 mmol) was treated in the same manner as above to produce 9-chloro-2-iodoacridine (**s12**) as a pale white solid. The product was used without further purification. (+)APCI-MS: m/z: 322 $[M+H]^+$. 9-Chloro-2-iodoacridine was further converted to the 2,9-diiodoacridine as described above to give the product as yellow solid (11 mg, yield 11%). ^{1}H NMR (800 MHz, Chloroform-*d*) δ 8.78 (d, *J* = 1.9 Hz, 1H), 8.34 (d, *J* = 8.8 Hz, 1H), 8.18 (d, *J* = 8.6 Hz, 1H), 8.00 (dd, *J* = 9.0, 1.9 Hz, 1H), 7.92 (d, *J* = 9.1 Hz, 1H), 7.84 (dd, *J* = 8.6, 6.5 Hz, 1H), 7.67 (dd, *J* = 8.8, 6.5 Hz, 1H). ^{13}C{^{1}H} NMR (201 MHz, $CDCl_3$) δ 148.8, 147.2, 141.7, 139.1, 133.1, 131.4, 131.3, 130.9, 130.0, 130.0, 128.4, 118.1, 94.2. HRMS (APCI), calcd. for $C_{13}H_8NI_2$: 431.8746 $[M+H]^+$, found: 431.8731.

1,7- and 2,6-dibromoacridines (s16 and **s17)**. 5-Bromo-2-((3-bromophenyl)amino)benzoic acid (**s13**) was synthesized using the same method as for 2-((3-iodophenyl)amino)benzoic acid. No NMR spectrum was collected due to its poor solubility. The crude product was vacuum dried and used as it was to produce 1,7- and 2,6-dibromoacridones (**s14** and **s15**) in the same manner as 1-

and 3-acridones. The total yield of the two steps was 25%. The mixture of the products was reduced as described in the general procedure to give pure 1,7- (yield 7%) and 2,6-dibromoacridine (yield 10%), both as light-yellow solids.

1,7-Dibromoacridine. ^{1}H NMR (800 MHz, Chloroform-*d*) δ 9.04 (s, 1H), 8.26 (d, *J* = 2.2 Hz, 1H), 8.19 (d, *J* = 8.7 Hz, 1H), 8.12 (d, *J* = 9.2 Hz, 1H), 7.89 – 7.84 (m, 2H), 7.65 (dd, *J* = 8.8, 7.1 Hz, 1H). ^{13}C{^{1}H} NMR (201 MHz, $CDCl_3$) δ 149.3, 147.7, 135.2, 134.7, 130.9, 130.5, 130.2, 130.0, 129.6, 127.7, 126.2, 122.0, 120.5. HRMS (APCI), calcd. for $C_{13}H_8NBr_2$: 335.9023 $[M+H]^+$, found: 335.8998, 337.8978, 339.8956.

2,6-Dibromoacridine. ^{1}H NMR (800 MHz, Chloroform-*d*) δ 8.67 (s, 1H), 8.44 (d, *J* = 1.9 Hz, 1H), 8.18 (d, *J* = 2.2 Hz, 1H), 8.10 (d, *J* = 9.2 Hz, 1H), 7.88 (d, *J* = 8.9 Hz, 1H), 7.86 (dd, *J* = 9.2, 2.1 Hz, 1H), 7.65 (dd, *J* = 8.9, 1.8 Hz, 1H). ^{13}C{^{1}H} NMR (201 MHz, $CDCl_3$) δ 149.3, 147.8, 135.1, 134.5, 131.7, 131.2, 130.2, 129.9, 129.3, 127.3, 125.3, 125.2, 120.2. HRMS (APCI), calcd. for $C_{13}H_8NBr_2$: 335.9023 $[M+H]^+$, found: 335.9003, 337.8998, 339.8991

1,7- and 2,6-diiodoacridines (a6a and **a8a)**. 1,7- and 2,6-dibromoacridines were treated similarly as 9-chloroacridine but with double amounts of reagents and doubled reaction time to give 1,7-diiodoacridine (yield 44%) as a pale yellow solid and 2,6-diiodoacridine (yield 58%) as a yellow solid.

1,7-Diiodoacridine. ^{1}H NMR (800 MHz, Chloroform-*d*) δ 8.89 (s, 1H), 8.56 (d, *J* = 1.9 Hz, 1H), 8.22 (dt, *J* = 8.7, 1.0 Hz, 1H), 8.18 (dd, *J* = 7.0, 1.0 Hz, 1H), 8.04 (dd, *J* = 9.1, 1.9 Hz, 1H), 8.00 (d, *J* = 9.1 Hz, 1H), 7.52 (dd, *J* = 8.7, 7.0 Hz, 1H). ^{13}C{^{1}H} NMR (201 MHz, $CDCl_3$) δ 149.1, 148.1, 139.9, 139.6, 137.7, 137.1, 131.4, 130.6, 130.5, 128.9, 128.3, 98.6, 92.2. HRMS (APCI), calcd. for $C_{13}H_8NI_2$: 431.8746 $[M+H]^+$, found: 431.8722.

2,6-Diiodoacridine. ^{1}H NMR (800 MHz, Chloroform-*d*) δ 8.72 (dt, *J* = 1.5, 0.6 Hz, 1H), 8.64 (d, *J* = 1.1 Hz, 1H), 8.43 (dt, *J* = 1.9, 0.6 Hz, 1H), 8.01 (dd, *J* = 9.1, 1.9 Hz, 1H), 7.96 (dt, *J* = 9.2, 0.7 Hz, 1H), 7.81 (dd, *J* = 8.8, 1.6 Hz, 1H), 7.74 (dt, *J* = 8.8, 0.6 Hz, 1H). ^{13}C{^{1}H} NMR (201 MHz, $CDCl_3$) δ 149.5, 147.8, 139.4, 138.7, 136.9, 135.0, 134.9, 131.1, 129.1, 128.2, 125.4, 97.7, 91.9. HRMS (APCI), calcd. for $C_{13}H_8NI_2$: 431.8746 $[M+H]^+$, found: 431.8724.

2,7-Diiodoacridone (s18). Acridone (100 mg, 0.51 mmol) was dissolved in 5 mL glacier acetic acid and iodine chloride (249 mg, 1.53 mmol) was added dropwise. The solution was refluxed for 6 h. The mixture was filtered while hot. The insoluble solid was washed with hot acetic acid (three times, 10 mL each). The remaining yellow solid was vacuum dried to give the product (134 mg, yield 59%). The insoluble product was used without further purification. HRMS (APCI), calcd. for $C_{13}H_8NOI_2$: 447.8695 $[M+H]^+$, found: 447.8675.

2,7-Diiodoacridine (a7a). 2,7-Diiodoacridone (105 mg) was treated as described in the general procedure to produce 2,7-diiodoacridine as a yellow solid (41 mg, yield 40%). ^{1}H NMR (800 MHz, Chloroform-*d*) δ 8.55 (s, 1H), 8.45 (d, *J* = 1.9 Hz, 2H), 8.02 (dd, *J* = 9.1, 1.9 Hz, 2H), 7.96 (d, *J* = 9.1 Hz, 2H). ^{13}C{^{1}H} NMR (201 MHz, $CDCl_3$) δ 147.8, 139.2, 136.9, 133.4, 131.1, 128.1, 92.2. HRMS (APCI), calcd. for $C_{13}H_8NI_2$: 431.8746 $[M+H]^+$, found: 431.8717.

COMPUTATIONAL METHODS

Molecular geometries for all species were optimized at the density functional (DFT) level of theory by using the correlation-consistent polarized valence-triple-ζ (cc-pVTZ) basis set.[30] The DFT calculations used the gradient-corrected exchange functional of Becke,[31] which was combined with the gradient-corrected correlation functional of Lee, Yang and Parr[32] (B3LYP). All DFT geometries were verified to be local minima by computation of analytic vibrational frequencies, and these (unscaled) frequencies were used to compute zero-point vibrational energies (ZPVE) and 298 K thermal contributions ($H_{298} - E_0$). All DFT calculations for the mono- and biradicals employed an unrestricted formalism. Total spin expectation values for Slater determinants formed from the optimized Kohn-Sham orbitals did not exceed 0.761 and 2.022 for doublet (monoradicals) and triplet (biradical) states, respectively. For singlet biradicals, the DFT "wave function" was allowed to break spin symmetry by using an unrestricted formalism.[33] Total spin expectation values for Slater determinants formed from the optimized Kohn-Sham orbitals in these cases ranged between 0.907 and 1.022, except for **q7** (0.000).

To improve the molecular orbital calculations for the (iso)quinolinium-based systems, dynamic electron correlation was also accounted for by using multi-reference second-order perturbation theory[34,35] (CASPT2) for multi-configurational self-consistent field (MCSCF) reference wave functions; these calculations were carried out for the DFT optimized geometries. The MCSCF calculations were of the complete active space (CASSCF) variety[36] and included (in the active space) the full π-space for each molecule and, for each of the mono- and biradicals, the nonbonding σ orbital(s). Some caution must be applied in interpreting the CASPT2 results since this level of theory is known to suffer from a systematic error proportional to the number of unpaired electrons.[37] Thus, the electronic energies are of the CASPT2/CASSCF(*m,n*)/cc-pVTZ//UB3LYP/cc-pVTZ variety (where *m* is the number of active electrons and *n* is the number of active orbitals), and estimates of the thermodynamic quantities, E_0 and H_{298}, are derived by adding to these electronic energies ZPVE and the sum of ZPVE and ($H_{298} - E_0$), respectively, where the latter are derived from the DFT calculations. Note that similar calculations for the acridinium-based systems were not possible due to their size.

In order to compute vertical electron affinities (EA_v) for the mono- and biradicals, single-point calculations (CASPT2/CASSCF(*m,n*)/cc-pVTZ for the (iso)quinolinium-based systems; UB3LYP/aug-cc-pVTZ[30,38] for the acridinium-based systems), using the UB3LYP/cc-pVTZ optimized geometry for each radical, were also carried out for the states that are produced when a single electron is added to the nonbonding σ orbital (or one of the two such orbitals) of each molecule.[39] Thus, for the monoradicals (doublet ground states) these calculations were carried out for (zwitterionic) *singlet* states, whereas for the biradicals (singlet ground states) calculations were carried out for (zwitterionic) *doublet* states.[40]

All CASPT2/CASSCF and DFT calculations were carried out with the MOLCAS 8.0[41 48] and Gaussian 09[42] electronic structure program suites, respectively.

ASSOCIATED CONTENT

Supporting Information. Plots of reaction efficiencies vs. S-T splittings of biradicals, calculated collision rate constants and measured second-order reaction rate constants for mono- and biradicals, synthesis schemes, NMR spectra, computational details. The Supporting Information is available

free of charge on the ACS Publications website.

ACKNOWLEDGEMENTS

We are grateful to the National Science Foundation (CHE-1464712) for financial support.

REFERENCES

(1) Alam, A. Md. The Advances and Applications of Arynes and Their Precursors to Synthesize the Heterocyclic Compounds: A Review. *Am. J. Heterocycl. Chem.* **2017**, *3*, 47–54.

(2) Romeo, R.; Giofre, S. V.; Chiacchio, M. A. Synthesis and Biological Activity of Unnatural Enediynes. *Curr. Med. Chem.* **2017**, *24*, 3433–3484.

(3) Wender, P. A.; Jeon, R. Bromoacetophenone-Based Photonucleases: Photoinduced Cleavage of DNA by 4‘-Bromoacetophenone−Pyrrolecarboxamide Conjugates. *Org. Lett.* **1999**, *1*, 2117–2120.

(4) Wenk, H. H.; Winkler, M.; Sander, W. One Century of Aryne Chemistry. *Angew. Chem. Int. Ed.* **2003**, *42*, 502–528.

(5) Williams, P. E.; Jankiewicz, B. J.; Yang, L.; Kenttämaa, H. I. Properties and Reactivity of Gaseous Distonic Radical Ions with Aryl Radical Sites. *Chem. Rev.* **2013**, *113*, 6949–6985.

(6) Wenthold, P. G.; Squires, R. R.; Lineberger, W. C. Ultraviolet Photoelectron Spectroscopy of the *o*-, *m*-, and *p*-Benzyne Negative Ions. Electron Affinities and Singlet−Triplet Splittings for *o*-, *m*-, and *p*-Benzyne. *J. Am. Chem. Soc.* **1998**, *120*, 5279–5290.

(7) Gao, J.; Jankiewicz, B. J.; Reece, J.; Sheng, H.; Cramer, C. J.; Nash, J. J.; Kenttämaa, H. I. On the Factors That Control the Reactivity of *meta*-Benzynes. *Chem. Sci.* **2014**, *5*, 2205–2215.

(8) Vinueza, N. R.; Archibold, E. F.; Jankiewicz, B. J.; Gallardo, V. A.; Habicht, S. C.; Aqueel, M. S.; Nash, J. J.; Kenttämaa, H. I. Reactivity of the 4,5-Didehydroisoquinolinium Cation. *Chem. – Eur. J.* **2012**, *18*, 8692–8698.

(9) Jing, L.; Nash, J. J.; Kenttämaa, H. I. Correlation of Hydrogen-Atom Abstraction Reaction Efficiencies for Aryl Radicals with Their Vertical Electron Affinities and the Vertical Ionization Energies of the Hydrogen-Atom Donors. *J. Am. Chem. Soc.* **2008**, *130*, 17697–17709.

(10) Max, J. P.; Ma, X.; Kotha, R. R.; Ding, D.; Milton, J.; Nash, J. J.; Kenttämaa, H. I. Reactivity of Organic σ,σ,σ,σ,σ-Pentaradicals. *Int. J. Mass Spectrom.* **2019**, *435*, 280–290.

(11) Kotha, R. R.; Yerabolu, R.; Ding, D.; Szalwinski, L.; Ma, X.; Wittrig, A.; Kong, J.; Nash, J. J.; Kenttämaa, H. I. Spin–Spin Coupling Between Two *meta*–Benzyne Moieties In a Quinolinium Tetraradical Cation Increases Their Reactivities. *Chem. – Eur. J.* **2019**, *25*, 4472–4477.

(12) Donahue, N. M.; Clarke, J. S.; Anderson, J. G. Predicting Radical−Molecule Barrier Heights: The Role of the Ionic Surface. *J. Phys. Chem. A* **1998**, *102*, 3923–3933.

(13) Ciampi, S.; Darwish, N.; Aitken, H. M.; Diez-Perez, I.; Coote, M. L. Chem. Soc. Rev. **2018**, *47*, 5146-5164.

(14) Vinueza, N. R.; Jankiewicz, B. J.; Gallardo, V. A.; LaFavers, G. Z.; DeSutter, D.; Nash, J. J.; Kenttämaa, H. I. Reactivity Controlling Factors for an Aromatic Carbon-Centered σ,σ,σ-Triradical: The 4,5,8-Tridehydroisoquinolinium Ion. *Chem. – Eur. J.* **2016**, *22*, 809–815.

(15) Logan, C. F.; Chen, P. *Ab Initio* Calculation of Hydrogen Abstraction Reactions of Phenyl Radical and *p*-Benzyne. *J. Am. Chem. Soc.* **1996**, *118*, 2113–2114.

(16) Stiles, M.; Miller, R. G.; Burckhardt, U. Reactions of Benzyne Intermediates in Non-Basic Media. *J. Am. Chem. Soc.* **1963**, *85*, 1792–1797.

(17) Gozzo, F. C.; Eberlin, M. N. 2-Pyridyl and 2-Pyrimidyl Cations: Stable o-Hetarynium Ions in the Gas Phase. *J. Org. Chem.* **1999**, *64*, 2188–2193.

(18) Wierschke, S. G.; Nash, J. J.; Squires, R. R. A Multiconfigurational SCF and Correlation-Consistent CI Study of the Structures, Stabilities, and Singlet-Triplet Splittings of *o*-, *m*-, and *p*-Benzyne. *J. Am. Chem. Soc.* **1993**, *115*, 11958–11967.

(19) Barfknecht, A. T.; Dodd, J. A.; Salomon, K. E.; Tumas, W.; Brauman, J. I. *Pure Appl. Chem*. **1984**, *56*, 1809-1818.

(20) Ma, X.; Jin, C.; Wang, D.; Nash, J. J.; Kenttämaa, H. I. Relative Reactivities of Three Isomeric Aromatic Biradicals with a 1,4-Biradical Topology Are Controlled by Polar Effects. *Chem. – Eur. J.* **2019**, *25*, 6355–6361.

(21) Jankiewicz, B. J.; Vinueza, N. R.; Kirkpatrick, L. M.; Gallardo, V. A.; Li, G.; Nash, J. J.; Kenttämaa, H. I. Does the 2,6-Didehydropyridinium Cation Exist? *J. Phys. Org. Chem.* **2013,** *26,* 707–714.

(22) Logan, C. F.; Chen, P. T. Ab initio Calculations of Hydrogen Abstraction Reactions of Phenyl Radical and *p*-Benzyne, J. *Am. Chem. Soc.* **1996,** *118,* 2113–2114.

(23) Roth, W. R.; Hopf, H.; Wasser, T.; Zimmerman, H.; Werner, C. 1,4-Didehydronaphthalin. *Liebigs Ann*. **1996**, 1691–1695.

(24) Kotha, R. R. Gas-Phase Reactivity Studies of Charged Quinoline Polyradicals by Using Distonic Ion Approach and Linear Quadrupole Ion Trap Mass Spectrometry, and Mechanistic Studies on Metal-Promoted Self-Assembly of Collagen Mimetic Peptides. Ph.D. Thesis, Purdue University, **2017**.

(25) Habicht, S. C.; Vinueza, N. R.; Archibold, E. F.; Duan, P.; Kenttämaa, H. I. Identification of the Carboxylic Acid Functionality by Using Electrospray Ionization and Ion-Molecule Reactions in a Modified Linear Quadrupole Ion Trap Mass Spectrometer. *Anal. Chem.* **2008,** *80,* 3416–3421.

(26) Su, T.; Chesnavich, W. J. Parametrization of the Ion–Polar Molecule Collision Rate Constant by Trajectory Calculations. *J. Chem. Phys.* **1982**, *76*, 5183–5185.

(27) Pedron, J.; Boudot, C.; Hutter, S.; Bourgeade-Delmas, S.; Stigliani, J.-L.; Sournia-Saquet, A.; Moreau, A.; Boutet-Robinet, E.; Paloque, L.; Mothes, E.; Laget, M.; Vendier, L.; Pratviel, G.; Wyllie, S.; Fairlamb, A.; Azas, N.; Courtioux, B.; Valentin, A.; Verhaeghe, P. Novel 8-Nitroquinolin-2(1H)-ones as NTR-Bioactivated Antikinetoplastid Molecules: Synthesis, Electrochemical and SAR Study. *Eur. J. Med. Chem.* **2018**, *155*, 135–152. https://doi.org/10.1016/j.ejmech.2018.06.001.

(28) Lee, J. A.; Roh, E. J.; Oh, C.-H.; Lee, S. H.; Sim, T.; Kim, J. S.; Yoo, K. H. Synthesis of Quinolinylaminopyrimidines and Quinazolinylmethylaminopyrimidines with Antiproliferative Activity against Melanoma Cell Line. *J. Enz. Inh. Med.l Chem.* **2015**, *30* (4), 607–614. https://doi.org/10.3109/14756366.2014.958082.

(29) Zhang, Y.; Guo, X.; Jia, L.; Xu, S.; Xu, Z.; Zheng, L.; Qian, X. Substituent-Dependent Fluorescent Sensors for Zinc Ions Based on Carboxamidoquinoline. *Dalton Trans.s* **2012**, *41* (38), 11776–11782. https://doi.org/10.1039/c2dt31139a.

(30) Dunning, T. H. Gaussian Basis Sets for Use in Correlated Molecular Calculations. I. The Atoms Boron Through Neon and Hydrogen. *J. Chem. Phys.* **1989**, *90*, 1007–1023.

(31) Becke, A. D. Density-functional Exchange-Energy Approximation With Correct Asymptotic Behavior. *Phys. Rev. A* **1988**, *38*, 3098–3100.

(32) Lee, C. T.; Yang, W. T.; Parr, R. G. Development of the Colle-Salvetti Correlation-Energy Formula Into a Functional of the Electron Density. *Phys. Rev. B*, **1988**, *37*, 785–789.

(33) (a) Polo, V.; Kraka, E.; Cremer, D. Some Thoughts About the Stability and Reliability of Commonly Used Exchange-Correlation Functionals – Coverage of Dynamic and Nondynamic Correlation Effects. *Theor. Chem. Acc*. **2002**, *107*, 291–303. (b) Gräfenstein, J.; Hjerpe, A. M.; Kraka, E.; Cremer, D. An Accurate Description of the Bergman Reaction Using Restricted and Unrestricted DFT: Stability Test, Spin Density, and On-Top Pair Density. *J. Phys. Chem. A* **2000**, *104*, 1748–1761. (c) Cramer, C. J. Bergman, Aza-Bergman, and Protonated Aza-Bergman Cyclizations and Intermediate 2,5-Arynes: Chemistry and Challenges to Computation. *J. Am. Chem. Soc.* **1998**, *120*, 6261–6269. (d) Gräfenstein, J.; Kraka, E.; Cremer, D. Density Functional Theory for Open-Shell Singlet Biradicals. *Chem. Phys. Lett.* **1998**, *288*, 593–602. (e) Crawford, T. D.; Kraka, E.; Stanton, J. F.; Cremer, D. Problematic *p*-Benzyne: Orbital Instabilities, Biradical Character, and Brojen Symmetry. *J. Chem. Phys.* **2001**, *114*, 10638–10650.

(34) Andersson, K.; Malmqvist, P.-Å.; Roos, B. O.; Sadlej, A. J.; Wolinski, K. Second-Order Perturbation Theory With a CASSCF Reference Function. *J. Phys. Chem.* **1990**, *94*, 5483–5488.

(35) Andersson, K. Different Forms of the Zeroth-Order Hamiltonian in Second-Order Perturbation Theory With a Complete Active Space Self-Consistent Field Reference Function. *Theor. Chim. Acta* **1995**, *91*, 31–46.

(36) Roos, B. O.; Taylor, P. R.; Siegbahn, P. E. M. A Complete Active Space SCF Method (CASSCF) Using a Density Matrix Formulated Super-CI Approach. *Chem. Phys.* **1980**, *48*, 157–173.

(37) Andersson, K.; Roos, B. O. Multiconfigurational Second-Order Perturbation Theory: A Test of Geometries and Binding Energies. *Int. J. Quantum Chem.* **1993**, *45*, 591–607.

(38) Kendall, R. A.; Dunning, T. H.; Harrison, R. J. Electron Affinities of the First-Row Atoms Revisited. Systematic Basis Sets and Wave Functions. *J. Chem. Phys.* **1992**, *96*, 6796–6806.

(39) Note that, for these calculations, we are computing the electron affinity of the radical site *not* the electron affinity of the *molecule*.

(40) Because the mono- and biradicals studied here contain a formal positive charge on the nitrogen atom, the state that is produced when an electron is added to the nonbonding orbital of any one of these species is formally zwitterionic; that is, it contains localized positive (π) and negative (σ) charges.

(41) (a) **MOLCAS 7.4**: Aquilante, F.; De Vico, L.; Ferré, N.; Ghigo, G.; Malmqvist, P.-°A.; Neogrády; Pedersen, T. B.; Pitonak, M.; Reiher, M.; Roos, B. O.; Serrano-Andrés, L.; Urban, M.; Veryazov, V.; Lindh, R. *J. Comp. Chem.* **2010**, *31*, 224–247. (b) **Code Development**: Veryazov, V.; Widmark, P.-O.; Serrano- Andrés, L.; Lindh, R. Roos, B. O. *Int. J. Quant. Chem.* **2004**, *100*, 626–635. (c) **MOLCAS 7**: Karlstrőm, G.; Lindh, R.; Malmqvist, P.-°A.; Roos, B. O.; Ryde, U.; Veryazov, V.; Widmark, P.-O.; Cossi, M.; Schimmelpfennig, B.; Neogrády, P.; Seijo, L. *Comp. Mat. Sci.* **2003**, *28*, 222–239.

(42) Frisch, M. J.; Trucks, G. W.; Schlegel, H. B.; Scuseria, G. E.; Robb, M. A.; Cheeseman, J. R.; Scalmani, G.; Barone, V.; Mennucci, B.; Petersson, G. A.; Nakatsuji, H.; Caricato, M.; Li, X.; Hratchian, H. P.; Izmaylov, A. F.; Bloino, J.; Zheng, G.; Sonnenberg, J. L.; Hada, M.; Ehara, M.; Toyota, K.; Fukuda, R.; Hasegawa, J.; Ishida, M.; Nakajima, T.; Honda, Y.; Kitao, O.; Nakai, H.; Vreven, T.; Montgomery, Jr., J. A.; Peralta, J. E.; Ogliaro, F.; Bearpark, M.; Heyd, J. J.; Brothers, E.; Kudin, K. N.; Staroverov, V. N.; Keith, T.; Kobayashi, R.; Normand, J.; Raghavachari, K.; Rendell, A.; Burant, J. C.; Iyengar, S. S.; Tomasi, J.;Cossi, M.; Rega, N.; Millam, J. M.; Klene, M.; Knox, J. E.; Cross, J. B.; Bakken, V.; Adamo, C.; Jaramillo, J.; Gomperts, R.; Stratmann, R. E.;Yazyev, O.; Austin, A. J.; Cammi, R.; Pomelli, C.; Ochterski, J. W.; Martin, R. L.; Morokuma, K.; Zakrzewski, V. G.; Voth, G. A.; Salvador, P.; Dannenberg, J. J.; Dapprich, S.; Daniels, A. D.; Farkas, O.; Foresman, J. B.; Ortiz, J. V.; Cioslowski, J.; Fox, D. J. Gaussian, Inc., Wallingford CT, 2013.